U
Universitetet
i Stavanger

FACULTY OF SCIENCE AND TECHNOLOGY

MASTER'S THESIS

Study programme/specialisation: Engineering Structures and Materials Specialisation: Structural engineering	Spring semester, 2018 Confidential
Author: Eirik Hartveit-Schee	*(signature of author)*

Faculty supervisor:
          Assoc. Prof. Ove K. Mikkelsen
External supervisor:
 	
          Atle Sjølyst-Kverneland, T. Kverneland & Sønner AS	

Title of master's thesis: Topology optimization of crane component	
Credits: 30 sp	

Keywords:
 	
     Topology optimization
     Crane
     SIMP
     WAAM
     Additive manufacturing
     FE analysis
	Number of pages: 77
	
	+supplemental material/other: 10
	
	Stavanger,......12/06/2018............
	                        date/year

Title page for Master's Thesis
Faculty of Science and Technology

Abstract

Topology optimization is an important tool for conceptual design of products. Finite element based topology optimization formulations, such as the Solid Isometric Material with Penalization (SIMP), have proved to be a solid algorithm for finding optimized geometries and have become widely implemented in commercial Computer Assisted Design (CAD) software. When topology optimization is viewed in conjunction with additive manufacturing (3D-printing), because of it's increased shape forming capabilities, highly optimized parts can be achieved. Technologies for 3D-printing large, metallic, load bearing structures is still in early development, but shows great promise, like the Wire Arc Additive Manufacturing (WAAM) method. These methods display advantages in other areas, such as material efficiency and fast deposition rate, that differentiate them from other, established 3D-printing methods.

Topology optimization was used to develop two conceptual designs of reduced volume compared to original component, which was an end truck of a over head crane system developed by T. Kverneland & Sønner AS (TKS). One design intended for traditional manufacture and one intended for additive manufacture.

Both proposed designs showed Von Mises stress above yield strength at certain areas of the model. Sharp corners and narrow radii of hole profiles were the main reason for this. Also, for the additive manufacture design, thin members were observed with high stress values. Designs could be improved by round-off of sharp corners, increasing radii of hole profiles and increasing thickness of thin members. It is believed that viable design can be achieved without drastic changes to the designs proposed in this thesis. Proposed design for traditional and additive manufacturing have a volume reduction of 17% and 14% respectfully relative to volume of original component.

Preface

This thesis is the conclusion to my master degree in Construction and Materials at the University of Stavanger (UiS), and was written during the spring semester of 2018.

The topic additive manufacturing have been a active research field during the author's five years of engineering studies. Reading about the innovation and application of this technology have been of great personal interest. I've always been curious about how the complex shapes seen in products produced by additive manufacturing were derived. This led to the field of topology optimization and, when choosing a topic for my master thesis, I expressed a wish for writing about these two fields. This resulted in a collaboration with T. Kverneland & Sønner AS (TKS) which took an interest to the thesis and agreed to provide material and guidance throughout this work.

The undersigned would like to express sincere gratitude to my supervisors, Assoc. Prof. Ove Kjetil Mikkelsen at UiS and Atle Sjølyst-Kverneland, Technical Manager at TKS, for their contributions to this thesis. I would also like to thank Thomas Kverneland at TKS for technical help regarding material provided by TKS, and to Adugna Deressa Akessa at UiS for technical help regarding work at computer lab.

Finally, I want to thank my dear wife, friends and fellow students for their companionship during my time studying at UiS.

Eirik Hartveit-Schee
Stavanger, 12.06.2018

Contents

List of Figures

Nomenclature

Roman Symbols

a Internal virtual work of an elastic body

E Stiffness

F Body force

f_y Yield stress

p SIMP penalty factor

t Traction force

U Space of kinematically admissible displacement fields

u Displacement of elastic equlibrium

V Volume

v Virtual displacement

Abbreviations

AM   Additive manufacturing

CAD   Computer aided design

DTU   Danmarks Tekniske Universitet

ESO   Evolutionary structural optimization

FE   Finite element

FEA   Finite element analysis

ISO   Isosurface

MBB   Messerschmitt-Bölkow-Blohm

MPN   Material Property Normalized

RAMP   Rational approximation of material properties

RHS   Rectangular hollow section

SIMP   Solid isotropic material with penalization

STL	Stereolithography
TKS	T. Kverneland & Sønner AS
TRL8	Technology Readiness Level 8
WAAM	Wire arc additive manufacturing

Greek Symbols

Γ	Boundary
γ_{M0}	Material safety factor
Ω	Domain
ρ	Density
σ	Stress
τ	Shear stress
Θ	Objective function
ε	Strain

Chapter 1

Introduction

1.1   Background

According to [1], topology optimization has become increasingly more present in the public's consciousness in recent years, and commercial-level CAD software companies now offer topology optimization for general consumption. [1] attributes this to the rise of additive manufacturing (AM) and it's ability to create shapes of great complexity. In particular interest for engineers, metal additive manufacturing is now seeing a substantial growth, with metal AM systems sold nearly doubling from 983 in 2016 to 1768 in 2017 [2]. TKS produce cranes and lifting applications for the heavy industry, and AM methods for manufacturing large, load bearing, metal components is of special interest to their activities. The mutual interest of the author and TKS into this field of technology comprise the background for the work presented in this thesis.

1.2   Target of thesis

The target is to use topology optimization to obtain a model of less volume compared to original component (presented in detail in section 3.3.1) and use this to develop two conceptual designs, one for traditional manufacture and one for additive manufacture. The aim is also to gain better understanding of the theoretical background for topology optimization, and gain better knowledge about WAAM, an additive manufacturing process for metals which could potentially be used to 3D-print the design intended for AM.

1.3   Delimitation of thesis

The literature study of topology optimization methods will focus mainly on those currently used in commercial software. The topology optimization will focus on the minimization of compliance under volume constraint formulation of a 3D continuum structure, and will be done in Abaqus 2017 with Tosca Structure. 3D-modeling both prior and after topology optimization will be done in Autodesk Professional Inventor 2017 (more information about software can be found in section 3.2). General yielding criteria of steel cross sections defined

in clause 6.2.1 of NS-EN 1993-1-1:2005 was used to select appropriate geometry from topology optimizations. S355 steel material strength was used (355 MPa). Computational power was limited by hardware available in computer lab at UiS.

Chapter 2

Literature review

2.1 Introduction

Before conducting the analysis part of this thesis it is of interest to get a better understanding of the theory and most popular methods currently being implemented in topology optimization. Also, wire arc additive manufacturing (WAAM) was deemed the most relevant additive manufacturing technique for producing large metal component, suited for the heavy industry and TKS. Therefore, a literature review will be done on these two topics.

2.2 Topology optimization

To limit the scope of this study, a series of question were formulated:

- Which topology optimization methods are being used in commercial software solvers?

- What is the theoretical foundation of these methods?

- Which of the previously mentioned methods are most prominent?

- Why are these methods more popular?

This section will attempt to answer these questions and thereby provide a good foundation for the work done in the analysis chapter. Preamble to this will be a short introduction to topology optimization and why it has become highly relevant with the introduction to 3D-printing technologies.

2.2.1 Introduction: Why do a topology optimization?

Eschenauer and Olhoff [3] writes in their extensive review of topology optimization of continuum structures that:

> The development and construction of products, especially in industrial practice frequently raises the question of which measures must be taken to improve the quality and reliability in a well-aimed manner without exceeding a certain cost limit.

They state that this question is the premise of an area in Computer Aided Engineering (CAD) known as *Structural Optimization*, and that the topology of a structure is crucial to it's optimality. They claim that traditionally, the topology of a design were chosen by the engineer from intuition, or by inspiration of previous designs. The structure could then undergo shape or sizing optimization, but the topology would remain unchanged. The power of topology optimization is that:

> ...the shape of external as well as internal boundaries and the number
> of inner holes are optimized simultaneously...[3]

Eschenauer and Olhoff claim that this makes topology optimization an important tool in the conceptual phase of design, given that the efficiency of a new product is often highly dependent on the choice of topology.

The field of topology optimization was first discussed in a paper by Australian engineer Anthony Michell in 1904, but it wasn't until the 1990s that it became a very active research field, after FE-based topology optimization formulations were being proposed, such as Bendsøe's SIMP method [4]–[6]. Advantageous with these FE optimization algorithms are that they have proven to be versatile and have been applied to design problems that are governed by different physical disciplines, such as solid mechanics, fluid dynamics and thermal dynamics [5]. Several (if not all) of the most prominent CAD software developers now offer FE-based topology optimization capabilities. The emergence of additive manufacturing technology is especially relevant to topology optimization and is discussed in section 2.3.

2.2.2 Topology optimization methods in commercial software

It has proven difficult for the author to find any definitive answers in literature about which topology optimization methods are being implemented in commercial software. Rozvany [4] writes in his review from 2009 of established methods of structural topology optimization that; to his knowledge all commercial FEA software apply the SIMP method, except for Tosca which he claims adopt an ESO method. He adds that there are indication that TOSCA might be switching to a SIMP approach as well. Deaton and Grandhi [7] later second this in their survey of structural topology optimization from 2014 and include TOSCA among the software which use a variant of the SIMP method. Investigation by the author into the Tosca topology module in Abaqus confirms that the SIMP method is used along with a method called RAMP.

Granted the general acceptance of the SIMP method in commercial software, there are other methods worth mentioning in this setting. Along with SIMP, reviews of topology optimization approaches [4], [7], [8] consider the following methods: Topological derivatives, level-set method, phase field method, evolutionary methods and biological inspired methods. These methods are still a subject of further research and could eventually be implemented in commercial software. On that point, Sigmund and Maute [8] have a interesting observation in their review:

> ...working on this review, the authors have become increasingly aware
> of how small the differences are between various topology optimiza-

tion approaches. In many cases it is even difficult to identify the novelty of a supposedly new approach.

They continue elaborating how variation of these different methods blend into each other and indicate that there is a lack of comparing different approaches in search for more efficient way to solve general topology optimization problems. They call for a reunion of efforts to finding an "optimal optimization approach".

Taking this into consideration, this thesis focus on the SIMP approach to topology optimization when deriving the theoretical background. For further investigation into the other methods previously mentioned; one can refer to the following literature:

- ESO/BESO - Huang, X., & Xie, M. (2010). *Evolutionary topology optimization of continuum structures : methods and applications.* Retrieved from:
  https://ebookcentral.proquest.com .

- Level set method - Wang, M.Y., Wang, X., Guo, D. (2003). *A level set method for structural topology optimization.* Retrieved from:
  http://www.sciencedirect.com/science/article/pii/S0045782502005595 .

- Topological derivative method - Norato, J.A., Bendsøe, M.P., Haber, R.B., Tortorelli, D.A. (2007). *A topological derivative method for topology optimization.* Retrieved from:
  https://link.springer.com/article/10.1007/s00158-007-0094-6 .

- Biological inspired method - Kobayashi, M.H., (2010) *On a biologically inspired topology optimization method.* Retrieved from:
  http://www.sciencedirect.com/science/article/pii/S1007570409002032 .

- Phase field method - Wallin, M., Ristinmaa, M., Askfelt, H. (2012). *Optimal topologies derived from a phase-field method.* Retrieved from:
  https://link.springer.com/content/pdf/10.1007%2Fs00158-011-0688-x.pdf .

2.2.3 Theoretical background

With increasingly more sophisticated software with continuously improved user interfaces, it becomes easier for inept users to obtain results from analysis. This can lead to unfortunate, or even critical, consequences if the analyst don't posses efficient understanding of the fundamentals regarding the problem and the tools used to solve it [9]. In an effort to avoid this, the following section will derive and explain the theory behind the SIMP approach which is used in the topology optimization in chapter 3. Fundamentals of the finite element method will not be considered in detail. The following subsections (section 2.2.3.1 to 2.2.3.3) are presented partially or directly as it appear in the first chapter of Bendsøe and Sigmund's book, [10].

2.2.3.1 Minimum compliance problem

In the pioneering paper [11]; Bendsøe and Kikuchi proposed the material distribution approach for finding optimal topology in continuum structures. In
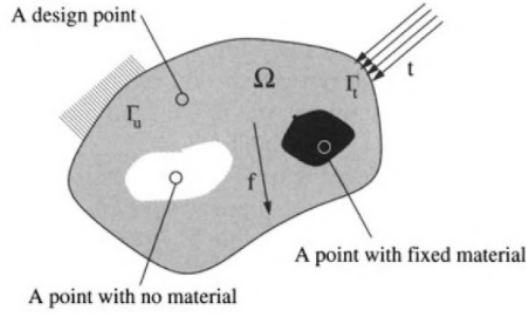
Figure 2.1: Generalized shape design problem of finding the optimal material distribution. [10]

this setting, a general definition of shape optimization is characterized as a determination for every point in a specified space if there should exist material in this point or not . This determination depends on a design objective and constraints. The following set-up for the optimal shape design will consider the objective of minimizing compliance (maximizing global stiffness) under volume constraint.

Consider a mechanical element as a body occupying a domain Ω_{mat}. This body finds itself inside a larger reference domain Ω (in R^2or R^3) defined such that it allows for the definition of loads and boundary conditions (illustration in fig. 2.1). This reference domain is often called ground structure, or in software, design space. Referring to Ω we can define the problem as finding the optimal choice of stiffness tensors E_{ijkl}. From the internal virtual work of an elastic body at the equilibrium u and for an arbitrary virtual displacement v:

$$a(u,v) = \int_\Omega E_{ijkl}(x)\, \varepsilon_{ij}(u)\, \varepsilon_{kl}(v)\, \mathrm{d}\Omega \,,$$

With linearized strains $\varepsilon_{ij}(u) = \frac{1}{2}\left(\frac{\partial u_i}{\partial x_j} + \frac{\partial u_j}{\partial x_i}\right)$ and the load linear form:

$$l(u) = \int_\Omega Fu\, \mathrm{d}\Omega + \int_{\Gamma_t} tu\, \mathrm{d}s \,,$$

the minimum compliance problem is defined as:

$$\min_{u\,\epsilon\, U,E} l(u) \quad \text{such that: } a_E(u,v) = l(u)\,, \quad \text{for all } v\,\epsilon\, U \,,$$

$$E\,\epsilon\, \mathbf{E}_{\mathrm{ad}}.$$

U is the space of kinematically admissible displacement fields, F are the body forces (designated as "f" in fig. 2.1) and t the traction forces. $\mathbf{E}_{\mathrm{ad}}$denotes the set of admissible stiffness tensors.

When using the finite element method the problem is discretized. If both E and u use the same finite element mesh the discrete form becomes:

$$\min_{u,E_e} \mathbf{F}^T\mathbf{u} \text{ such that: } \mathbf{K}(E_e)\mathbf{u} = \mathbf{F} \,,$$

$$E_e \, \epsilon \, \mathbf{E}_{\mathrm{ad}} \, .$$

$\mathbf{u}$ and $\mathbf{F}$ are the displacement and load vectors respectfully. E_e is the stiffness in element e, the stiffness matrix $\mathbf{K}$ depends on E_e in the following way:

$$\mathbf{K} = \sum_{e=1}^{N} \mathbf{K}_e(E_e) \, ,$$

where $\mathbf{K}_e$ is the global level element stiffness matrix and N is the total number of elements.

2.2.3.2 Design parametrization and SIMP

Previously, the optimization considered every point in the reference space Ω. In a finite element formulation this now becomes a determination for every *element* in Ω. An element is either a solid material element (1) or a void element (0). The solid elements define the subset Ω_{mat}. The goal is to find the optimal arrangement of solid elements, i.e. the optimal subset Ω_{mat}. The output can be imagined as a black and white raster representation of the optimal geometry. The approach above implies that $\mathbf{E}_{\mathrm{ad}}$ consist of the stiffness tensors which:

$$E_{ijkl} = 1_{\Omega_{mat}} E^0_{ijkl}, \ 1_{\Omega_{mat}} = \left\{ \begin{array}{ll} 1 & \text{if } x \, \epsilon \, \Omega_{mat} \, , \\ 0 & \text{if } x \, \epsilon \, \Omega \backslash \Omega_{mat} \, , \end{array} \right. \tag{2.1}$$

$$\int_{\Omega} 1_{\Omega_{mat}} \mathrm{d}\Omega = \mathrm{Vol}(\Omega_{mat}) \leq V \, .$$

Here the volume constrain is implemented by a limit, V, which is set by the designer. In software this limit is often defined as a fraction of the design space volume. E^0_{ijkl} is the stiffness tensor for the given isotropic material.

Solving the discrete problem is difficult. Dual methods, simulated annealing and genetic algorithms are attempts to solve this, but for large scale problems, involves prohibitive computational efforts. The most common way to solve the discrete optimization problem is to replace $1_{\Omega_{mat}}$ with a continuous variable $\rho(x)$ $(0 \leq \rho(x) \leq 1, \, x \, \epsilon \, \Omega)$. This allows for elements to have intermediate density values, which makes little sense in a physical setting. Therefor, a penalty is introduced to intermediate values in an effort to direct the solution to one mostly consisting of 1 and 0 values. Shortly after the publication of [11], Bendsøe followed up with a method of such penalizing. This method was later termed SIMP by Rozvany et. al in [12], and has proven to be very efficient and popular. In SIMP formulation, 2.1 becomes:

$$E_{ijkl} = \rho(x)^p E^0_{ijkl} \, , \quad p > 1 \, , \quad \int_{\Omega} \rho(x) \, \mathrm{d}\Omega \leq V \, . \tag{2.2}$$

The density interpolates between 0 and E^0_{ijkl}:

$$E_{ijkl}(\rho = 0) = 0 \, , \qquad E_{ijkl}(\rho = 1) = E^0_{ijkl} \, ,$$

The penalty in the form of the exponent p make intermediate values unfavorable when p is larger than 1, because the stiffness contribution of the element decreases while the volume contribution is unchanged, making it "uneconomical" and therefore less likely to appear in the optimal design. A p value of ≥ 3 is usually required to obtain "0-1" designs.

Figure 2.2: Dependence of the optimal topology on mesh refinement for the MBB-beam example. Solution for a discretization with a) 2700, b) 4800 and c) 17200 elements. [10]

2.2.3.3 Complications

Mesh-dependency Mesh-dependency is a problem which is not addressed with the SIMP scheme. The dependency leads to a lack of existence of solutions to the distributed problem. Optimally, a refinement of the finite element mesh should result in a more detailed or smoother representation of the same geometry obtained with rougher meshes, but as illustrated in fig. 2.2[1], the refinement leads to a more detailed and qualitatively different structure . The reason for this is that the introduction of new holes without changing the volume generally increase the efficiency of the structure with respect to the objective function. The way to solve this is to implement some restriction to the variation of density, effectively ruling out the possibility of forming finer structures. Three ways of introducing such restrictions exist: adding constraints to the optimization problem, directly reducing the parameter space for designs or applying filters. Examples include perimeter control, where an upper bound to the total amount of perimeter length of the holes created are defined; filtering density, limitations to the density distribution; or filtering sensitivity, element sensitivities are modified by a weighted average of element sensitivities in a fixed neighborhood of elements.

Checkerboard The problem with formation of checkerboard patterns in the mesh is not a real issue for macroscopic problems if the problem of mesh-dependency have been taken into account. The checkerboard formation appear because certain discretized formulations of topology design overestimate the stiffness contribution of this pattern. This is an error stemming from the FE method, rather than the SIMP method [4].

Non-uniqueness and local optima Most problems in topology optimization are not convex, and several local minima might be present. Also, an optimization might have several optima like uni-axial tension design, where one thick bar works just as well as several thinner bars with the same overall area. To ensure a stable convergence towards reliably good designs a procedure know

---

[1]The optimization of a support beam from a civil air-craft produced by Messerschmitt-Bölkow-Blohm (MBB) has become a classical example problem in topology optimization and referred to as the MBB-beam.[13]
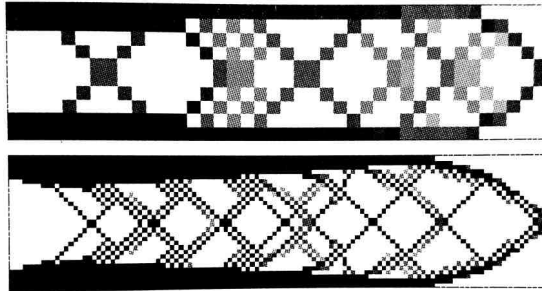
Figure 2.3: The checkerboard problem. [10]

as the continuation method should be used. The method is simply to start the optimization with a penalty parameter of $p = 1,0$ and let it converge. Then increase p by some $\triangle p$ and run the optimization again and continue this procedure until the output is of a satisfactory "1-0"-form (previously mention to be $p \geq 3$). This ensures that the solution doesn't move too far from the global optimum.

2.2.4 Why is SIMP so prominent in commercial software?

Deaton and Grandhi [7] credit the relative simplicity of SIMP for it's widespread use in commercial software. Rozvany [4] elaborate on why SIMP is generally accepted as the "go-to" method for topology optimization in commercial software. He bring up the importance of the efforts done by the topology optimization group at DTU for explaining the SIMP method to the international community. Especially the educational article, [14], by Sigmund, which describe a 99-line SIMP-code in Matlab. Sigmund, together with Tcherniak, also released a free web-based topology optimization program using SIMP in the hopes of introducing topology optimization to a broader range of engineers and students. The software providing topology optimization capabilities at the time were expensive and required lengthy education of the operator, and this web-application could serve as a starting point for learning more about, and gain insight in the method [15]. The website (*http://www.topopt.dtu.dk/*) have gone through some changes since 2001. It now offers apps for Android and iOS for both 2D and 3D topology optimization and, in the author's opinion, worth a look for a person new to this field and offers an intuitive way of understanding the effect of the parameters in SIMP.

Rozvany also highlights the fact that [10], which mainly use SIMP, have such a strong position in topology optimization literature and a factor why this method gained a "complete acceptance" in commercial software [4]. A general statement for the prominent use of SIMP is that it is a relative simple method which yield good results, even without the extra considerations mentioned in section 2.2.3.3 [3].

9

2.3 Wire and Arc Additive Manufacturing

2.3.1 Introduction

Additive manufacturing (AM), or 3D-printing technologies have undergone a rapid development in recent years, especially on printing metallic components, which is often more relevant for engineering purposes [16]. The main advantage of additive manufacturing is the freedom it provides to the designer. Therefore, topology optimization and additive manufacturing is a promising combination for producing highly optimized parts [17]. The geometry produced by topology optimization procedures is often complex and difficult (sometimes impossible) to manufacture by traditional methods. There are efforts being made to make topology optimization software consider traditional manufacturing limitations. However, the research of both additive manufacturing and topology optimization should be closely tied to realize the full potential of these fields [5].

Taken this into account, the thesis will include a section about the state-of-the-art of the wire arc additive manufacturing method. Area of focus will be the resulting microstructure of parts produced with WAAM and the process parameters which control this.

2.3.2 Why WAAM?

Ding et al [18] explains the different methods for additive metal manufacturing. Technologies are classified into two groups; powder-feed or wire-feed. A powder-feed process provides high geometrical accuracy on small parts, but the use of fine powder can potentially be a safety concern for operators. Wire-feed methods are a more environmental friendly process with a high material usage efficiency, up to 100% (the term "high buy-to-fly ratio"[2] is often used). [18] also says that metal wires are cheaper than the metal powder used in AM, and that makes wire-feed technology more cost-competitive.

[18] continues, wire-feed processes are grouped with respect to energy source used. Three main groups exist; laser based, electron beam based and arc welding based. Arc welding have some important advantages, namely a higher deposition rate, energy efficiency and lower cost. As a result, WAAM is a promising manufacturing technology and is being developed as the method of choice for large-scale metallic structures [20]. Therefore, it was deemed the most relevant AM technology for TKS and their activities in the heavy industry and it is of interest to gain knowledge about this topic.

2.3.3 General WAAM setup

WAAM is layer-by-layer arc welding method of producing metallic parts. Most commercial progress in this field has been made by Norsk Titanium (Norway), which reached TRL8[3] maturity with their MERKE IV machine. Other machine manufacturers recently launched new WAAM solutions, like Addilan (Spain), Mazak Corporation (Japan) with VARIAXIS j-600AM and Mutoh Industries

---

[2]Term from the aerospace industry used to describe the ratio between material purchased to manufacture part vs. material of finished part.[19]

[3]Technology Readiness Level 8: measurement system developed by NASA to determine the maturity level (1-9) of a particular technology.[21]

1. Computer
2. Control Cabinet
3. Welder
4. Robot
5. Torch
6. Laser profiler
7. Work piece
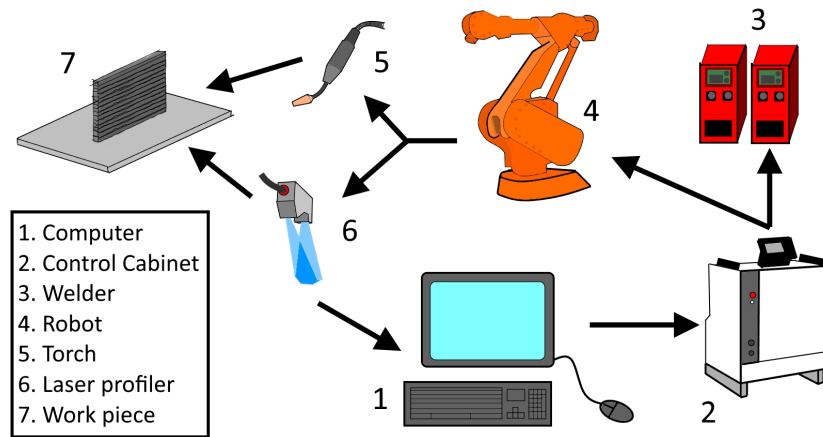
Figure 2.4: Schematic diagram of the experimental WAAM system (author's edit of figure seen in [18])

(Japan) with Value Arc MA5000-S1[22]. In all of these cases, the manufacturing process is contained within an inert gas chamber of a set size. This is because of titanium's stringent gas shielding requirements [23]. For more freedom in terms of part size and the ability to implement other manufacturing processes, out-of-chamber systems must be used[24]. Taking the size of TKS produced components into account, out-of-chamber solutions was deemed most relevant and will be of focus in this literature study.

It has not been possible for the author to find examples of commercially available, out-of-chamber WAAM systems. Academic research show some examples of experimental out-of-chamber systems [16], [18], [24]–[27]. In particular the work done at Cranfield University shows great potential, which, along with published research in the field, run the very informal https://waammat.com website about WAAM technology. Also worth mentioning is MX3D's very ambitious WAAM manufactured bridge in Amsterdam. Although detailed technical information could not be found regarding their WAAM system, MX3D claim great progress and expect to be done printing the entire bridge in early 2018 [28].

An illustration of a general WAAM system can be found in fig. 2.4 . It consists of a weld torch, apparatus for movement of torch, wire feed, substrate, control module for welding equipment and a computer to gather input and steer the process. To increase control of process parameters, additional monitoring devices have been used, including temperature measurement [16], [25], laser profilers (measuring of dimensions) [18] and measurements for oxygen levels [22]. Using turntable to rotate the substrate have also been proposed for further flexibility in movement [16].

Welding techniques The arc welding process can be based on either tungsten inert gas (TIG), metal inert gas (MIG) or plasma arc welding (PAW). MIG is the preferred process because the coaxiality between the welding torch and the consumable wire makes for easier tool paths [23]. Many researches implement the cold metal transfer (CMT) technology from Fronius in their WAAM system[16], [25], [29]. CMT is a modified MIG process which provides the same

11
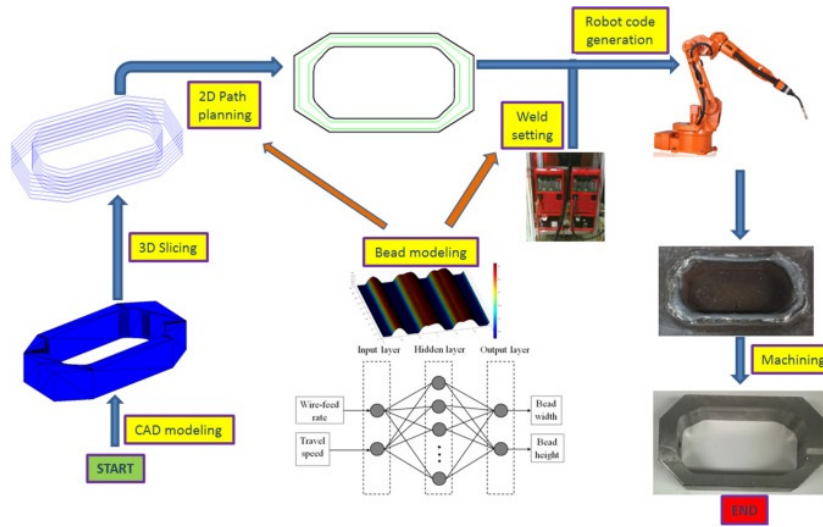
Figure 2.5: Automated process planning for robotic WAAM system. [31]

material deposition as MIG with less welding current, resulting in lower thermal input [30]. This is advantageous for AM because the realizable wall thicknesses are mainly determined by the heat input [16]. Also, the use of CMT can reduce other issues related to heat accumulation and are highlighted in section 2.3.5.

Movement apparatus   The options for moving the weld torch is either by a gantry machine or a robotic arm. For out-of-chamber systems robotic arm is mostly used. Robotic arm usually provides more degrees of freedom in movement than a gantry machine would. Ideally, the path planning of the robot is derived automatically from a CAD model of the part being manufactured. The 3D-model is sliced into layers, then a 2D path is created for every layer, taking weld bead modeling into account the code for the robot arm is created [31]. An illustration of the automated process is shown in fig. 2.5 .

Other implementations   WAAM produces near net-shaped geometries which means that further machining is often required to obtain satisfactory shape and surface of part[27]. Efforts have been done to implement these finishing procedures as in-process instead of post processing. [32], [33] implemented surface milling on the top and sides of the beads after each deposited layer, this reduces the milling difficulty but is quite time consuming. A known issue is the anisotropic behavior of metals produced with WAAM. To improve the microstructure pressure rolling have been implemented in various ways in experimental WAAM setups. [34] implemented a profiled roller pass between each layer; and [35] mounted a mini-roller close to the weld torch which continuously rolled the deposited layer. To prevent oxidation of welded metals, especially titanium, [24] developed a local gas shielding system mounted on the weld torch for use in out-of-chamber systems.
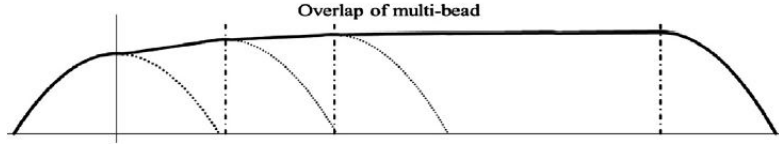
Figure 2.6: Unstable overlapping behavior. [18]

2.3.4 Process parameters

AM processes usually involve many process parameter that need to be optimized and WAAM is no different. To achieve specific wall dimensions several parameters have proven dominant; parameters such as wire feed speed, travel speed (of torch), arc length, interpass temperature, wire feed angle, gas flow and welding power supply parameters. Selecting optimized values of these parameters are highly important for the end result [36]. More specifically this relates to the control of single weld bead geometry and the overlapping of these beads, which has significant effects on surface quality, dimensional accuracy and mechanical properties of metallic parts produced in this way[37].

[22], [29], [38] developed experimental WAAM systems and optimized the process parameters considering bead geometry through trial and error. Although this might be sufficient in early development, establishing robust prediction models to gain effective control over the manufacturing process are necessary for the development of a automated WAAM system [26]. Several methods have been used in this effort. [26] used the response surface method (RSM) to create a second-degree polynomial model for the prediction of bead height and width considering weld current, travel speed and wire feed speed as input parameter. Due to the assumptions involved in RSM, [36] argues that genetic programming are better suited for establishing general prediction models. [36] developed two such models and compared the ability to predict bead geometry. Here, peak current and travel speed were found to be most influential for bead height, while bead width was most influenced by peak current and wire feed speed.

An optimized overlapping model is important to avoid unstable layer thickness (fig. 2.6) , which errors can accumulate on subsequent layers [18]. To predict overlapping behavior of weld beads, one should first establish a model for approximating bead profile. [37] compared familiar mathematical profile models such as circular arc, parabola and cosine function (fig. 2.7a) to measured bead dimensions of different welding parameters. It was shown that suitability of profile model was dependent on the ratio of wire feed speed to travel speed. Here, only bead height and width were considered. To improve the profile model and establish a prediction model for overlapping, [18] also considered cross-sectional area of bead. Parabola and cosine functions were shown to be most accurate. Using the parabola approach, an overlapping model was developed by defining a critical valley with an "overlapping tangent" (see fig. 2.7b). The critical valley defines a minimum center to center distance $d*$ for weld beads necessary for a stable overlapping process.

13

(a) Examples of bead profile models.
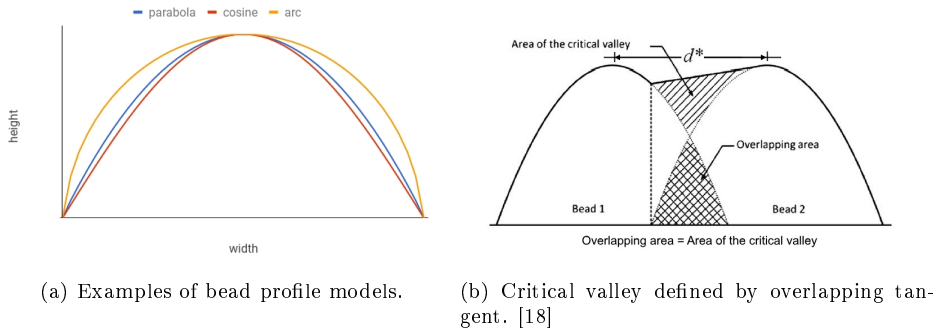
(b) Critical valley defined by overlapping tangent. [18]

Figure 2.7: Weld bead and overlapping models.

2.3.5 Microstructure of metal from WAAM

AM have gone form being a prototyping technology to becoming the actual production method. Important for this switch is that proper material properties can be ensured. A lot of work have been done on the research of microstructures in metals produced by WAAM. Several different metals have been successfully deposited with WAAM technology; titanium, aluminium, steel, invar, brass, copper and nickel [23]. Among these, most of the investigative efforts have gone into the Ti-6Al-4V alloy, and is attributed to the strong business case that can be made for complex, low production volume titanium parts [39]. As mentioned earlier, titanium alloys require stringent gas shielding, which, for out-of-chamber systems, is hard to achieve properly. Because of this, and due to the relevance for TKS, microstructure of steel alloys will be of focus in this thesis.

The most notable difference between traditional production methods and WAAM are arguably the nature of the thermal strains of the two methods. While traditional wrought alloys undergo a uniform thermal processing, different layers in the AM process are subjected to different numbers of thermal cycles (fig. 2.8) . Consequentially, the AM component are expected to consist of different microstructures and properties than that of wrought alloy [20]. [20], [25], [40], [41]observed this phenomenon. Microstructural components vary with different steel alloys, but generally, a columnar grain growth perpendicular to the substrate (upwards) can be observed [20], [40]. This is similar to what is seen in traditional welding microstructures [42]. The growth direction is a result of the temperature gradient created the multi-pass welding. The existence of layer bands results, to a varying degree, in an anisotropic behavior, with higher tensile strength in the horizontal direction compared to the vertical where the layer bands occur [20].

[20] studied the microstructure of a maraging steel thin-wall component manufactured by WAAM. They observed that the bottom layers consisted of long columnar dendritic grains with austenite retained between dendrites, while at the top, the grains were less columnar with little austenite observed (shown in fig. 2.9) . This difference in microstructure from early deposited layers to top layers affect the mechanical properties, and [20] observed brittle regions in the early layers while getting softer towards the top layers. [20] also compared microstructure of as-deposited and heat treated maraging steel produced by WAAM. They showed that heat treatment of the component eliminated the
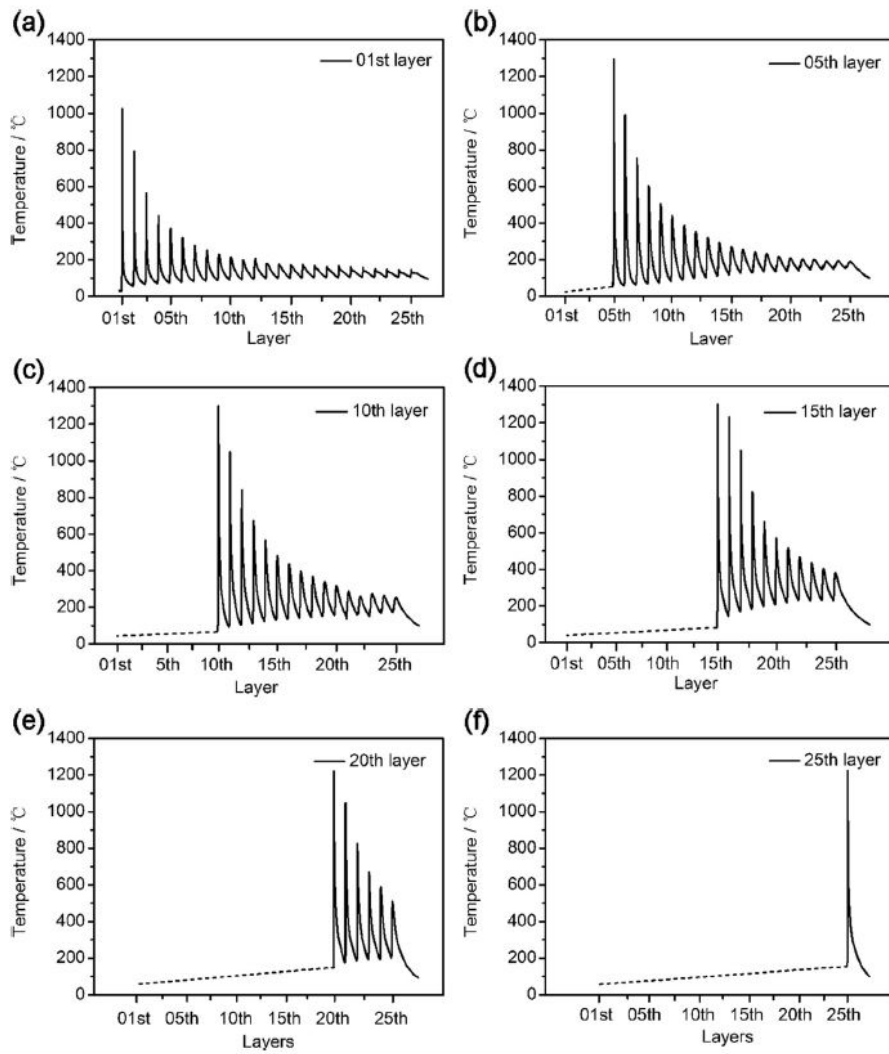
14

Figure 2.8: Thermal history of layers: (a) 1st; (b) 5th; (c) 10th; (d) 15th; (e) 20th; (f) 25th (last). [25]
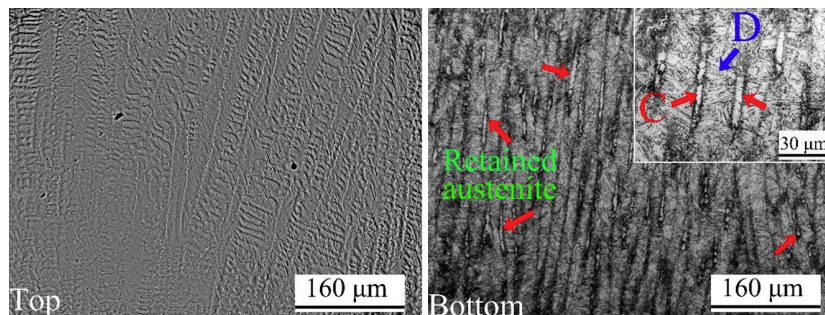

Figure 2.9: Microstructure of WAAM maraging steel. [20]

difference in mechanical properties from bottom to top layer and decreased the anisotropy.

The temperature gradient also introduce distortion, which affects precision, and residual stresses which is negative for mechanical performance. As mentioned earlier, [34] implemented high-pressure rolling in various ways in an effort to improve these issues. Although total deposition time naturally increased, they observed reduction in both distortion and residual stresses while also refining grain size. Additionally, the previously mentioned CMT technology have been implemented in several experimental WAAM setups ([16], [25], [29]) to reduce the heat input and show promising results on improving issues attributed to heat accumulation.

2.3.6   Designing for WAAM

Although a lot can be done to improve and optimize WAAM as a production method, one should also look at the possibilities of improving part designs to better accommodate for WAAM's unique capabilities. The work done at Cranfield University have been important for the development of WAAM as a commercial technology. One of those efforts is the article by Lockett et al. [19] which propose an initial set of design rules for WAAM. Some of these design rules will be highlighted below.

Lockett et al.[19] says WAAM is more restricted when it comes to freedom in design than other 3D-printing methods. However, there are some unique possibilities with WAAM as well, such as building overhanging structures without supports and use of a part-rotator to change the building orientation during deposition. A successful WAAM manufacture should consider build orientation, build sequence and design constraints.

Symmetry   As discussed earlier, components produced by WAAM can be subject to distortion due to the thermal strains from heating and cooling, which build up residual stresses. Utilizing a symmetrical deposition strategy can balance this build up and prevent distortion during manufacture. By placing the substrate in a plane of symmetry (or partial symmetry) and rotating it between each layer, the part can be created by depositing layers alternately on each side of the substrate. It is also possible, if the part does not have any suitable symmetry planes, to create two parts "back to back". These parts must be heat treated before separation to relieve residual stresses. Fig. 2.10 shows an example part and fig. 2.11 illustrates different possibilities in placing of the substrate (note that these are not equally optimal).

Unfinished faces   Not all faces of a component requires post-machining, but the as-deposited surface may have stress raising features which might require special consideration, especially in fatigue driven parts.

Machining   When post-machining is required, standard design for machining guidelines should be followed. If the WAAM system have integrated machining, the part can be machined between at every layer or another given interval. Careful consideration must be taken to ensure accessibility. An allowance for machining must be added to the faces, this is typically 1 mm.

16
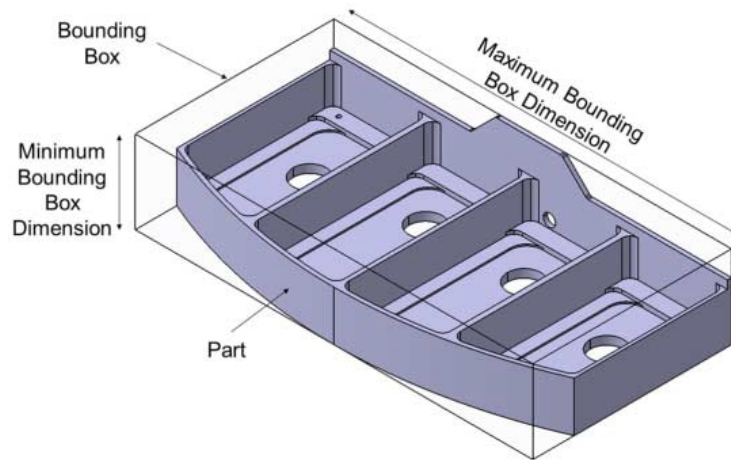
Figure 2.10: Example part. [19]
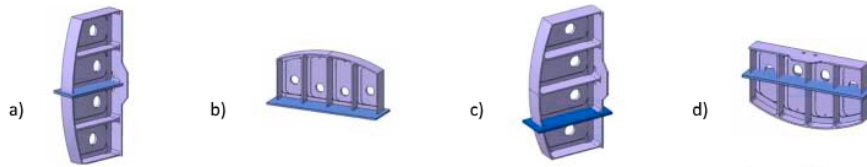
Figure 2.11: Different substrate positions (blue plate): a) Central Web on Plane of Symmetry; b) Planar Outer Wall; c) Planar Internal Wall; d) Plane of Symmery or Partial Symmetry (Not Aligned with a Wall). [19]

Undesirable features WAAM is not recommended for manufacturing complex 3D parts, in contrast to other AM methods. In addition to avoiding complexity, long thin unsupported members may be difficult to deposit and post-machine and should also be avoided.

Corners External and internal radii at corners are preferred. While avoiding the stress raising properties of sharp edge it also allow for continuous deposition around the corners.

Chapter 3

Topology optimization analysis

3.1 Introduction

In this study several topology optimization analyses were performed. The goal of these analyses was to find the level of volume reduction, relative to the original component (seen in fig. 3.3), that could be achieved without violating the general elastic yielding criterion stated in NS-EN 1993-1-1:2005 clause 6.2.1 (Eurocode 3) [43]. Values for the relevant stresses of yielding criteria was obtained from static FE-analysis of the last iteration of the topology optimization routine taken at a chosen critical point. The critical point was determined to be located at area where maximum Von Mises-stress of said analysis could be observed.

The topology with the largest volume reduction which satisfies the previously mention yielding criteria was used as a conceptual design guideline for two different manufacturing situations. The first was intended for traditional manufacturing methods available to TKS. The second was intended for additive manufacturing. The resulting models for these two design cases would under go a standard FE-analysis, in an effort to obtain a basic validation of the results.

3.2 Software

Two software solutions for topology optimization was available to the author; either the *Ansys* with the *Topology Optimization ACT*[1] *extension* or *Abaqus FEA 2017* with *Tosca Structure*. After preliminary tests of the two, Abaqus was chosen. Analysis was preformed with Abaqus CAE 2017. For 3D-modeling of the design space, Autodesk Inventor Professional 2017 was used (further references to this software will be called "Inventor"). Some basic information about the programs used is presented below.

Abaqus[2]   A software suite for finite element analysis developed by Dassault Systèmes as a part of their analysis and simulation brand, Simulia. The Abaqus

---

[1] *Application Customization Toolkit.*
[2] Ref: https://www.3ds.com/products-services/simulia/products/abaqus/

software suit consist of four core products:

- CAE, or "complete abaqus environment", used for modeling, pre-processing and visualizing finite element analysis results.

- Standard, general-purpose finite element analyzer.

- Explicit, special-purpose finite element analyzer.

- Multiphysics, finite element analyzer for dynamics of different field such as fluid, thermal, electrical and acoustics.

Recently had it's own topology optimization module, referred to as ATOM, replaced by Tosca Structure.

Tosca[3][4] Tosca is an optimization software suite originally developed by FE Design. FE Design was acquired by Dassault Systèmes in 2013 and Tosca became the optimization suite for the previously mention Simulia product package. Tosca consist of two products, namely Tosca Fluid, for design of fluid flow systems; and Tosca Structure, which offers structural optimization routines for topology, shape, bead and sizing.

Inventor[5] Inventor is a 3D CAD software for mechanical design, documentation and product simulation. Developed by Autodesk.

3.3 Preparation for analysis

3.3.1 Original part provided by TKS

The part subjected to topology optimization in this thesis is the end truck of an overhead crane system developed by TKS. Overhead crane and end trucks can be seen in fig. 3.1 . The overhead crane has a span of 14 meters and a lifting capacity of 10 000 kg. More information regarding the overhead system can be found in appendix A.1. The end truck assembly (fig. 3.2) contains several components and the main focus for analysis will be on the beam-like structure of the end truck shown in fig. 3.3. The beam consists of a 2,18 m long rectangular hollow section (RHS) with two steel plates welded to each end.

3.3.2 Drafting design space

The design space was developed from the original part by the author. This work was done in Inventor. In an effort to make use of the freedom in manufacturing which WAAM provides, the design space was formed to encompass both the RHS part and the steel plates as one continuous object. Some aspects of the original component were kept unchanged. Span length of 2,5 m between center of wheel holes; Outer dimensions of the RHS (150 mm x 250 mm); and wheel hole dimensions (ø 40). Considerations were taken to ensure that the design space would not interfere with the original wheels or the runway rails.
    The different drafts towards the final design can be seen in fig. 3.4 . The

---

[3]Ref: https://www.3ds.com/products-services/simulia/products/tosca/
[4]Ref: https://en.wikipedia.org/wiki/Dassault_Systemes
[5]Ref: https://www.autodesk.com/products/inventor/overview
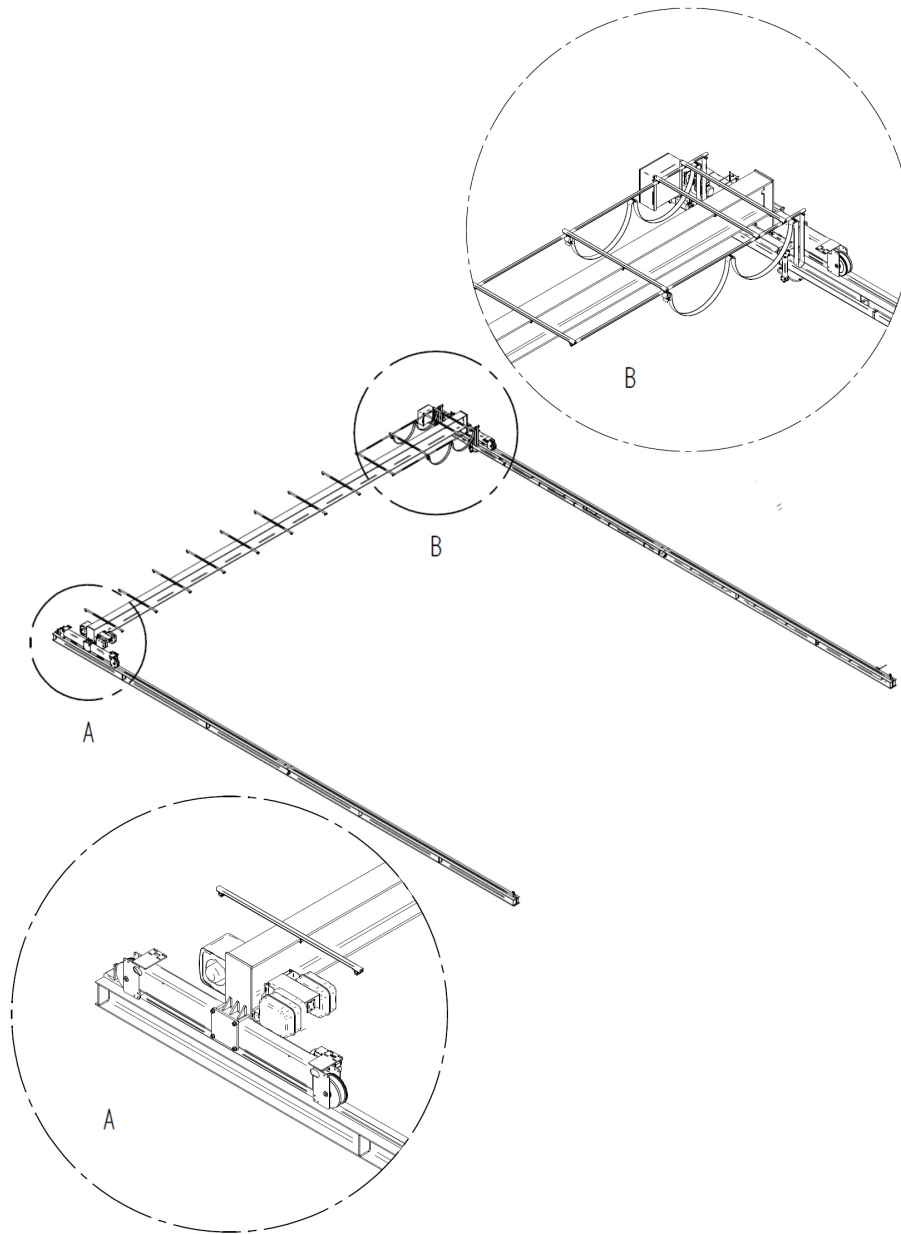
Figure 3.1: Overhead crane. End trucks are located at A and B.
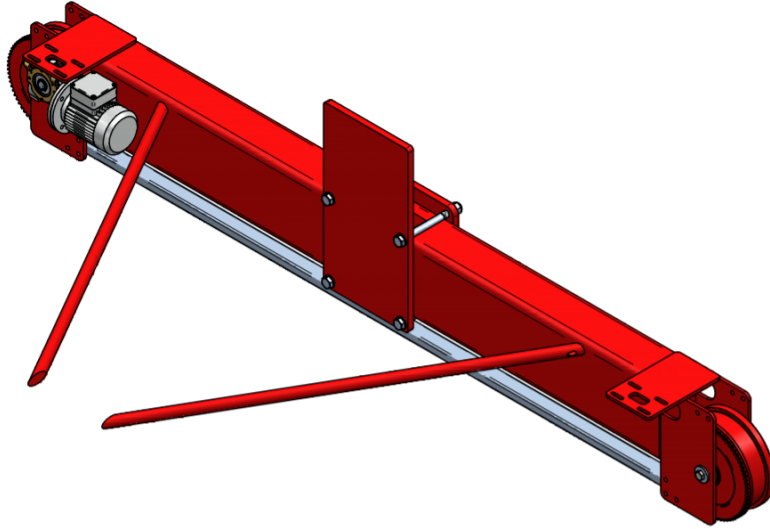
Figure 3.2: End truck assembly.
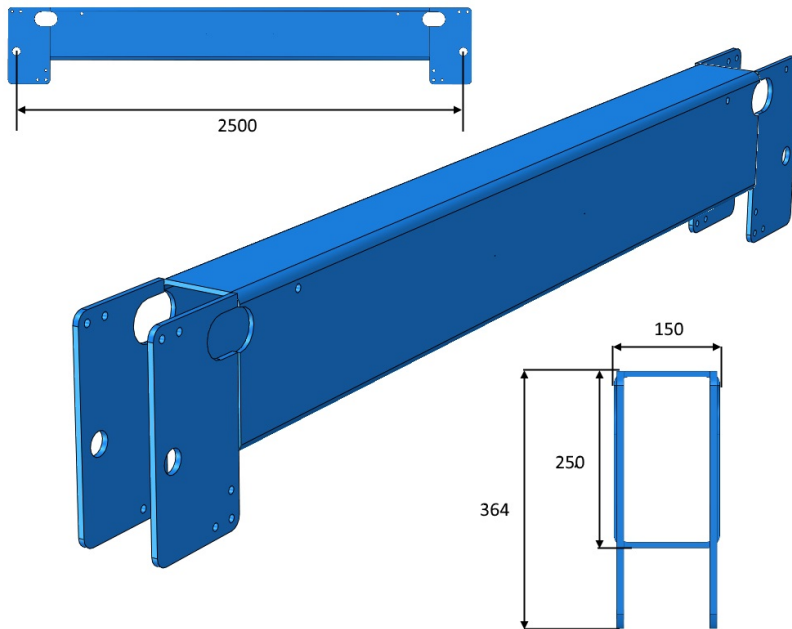
Figure 3.3: Beam part of end truck assembly.
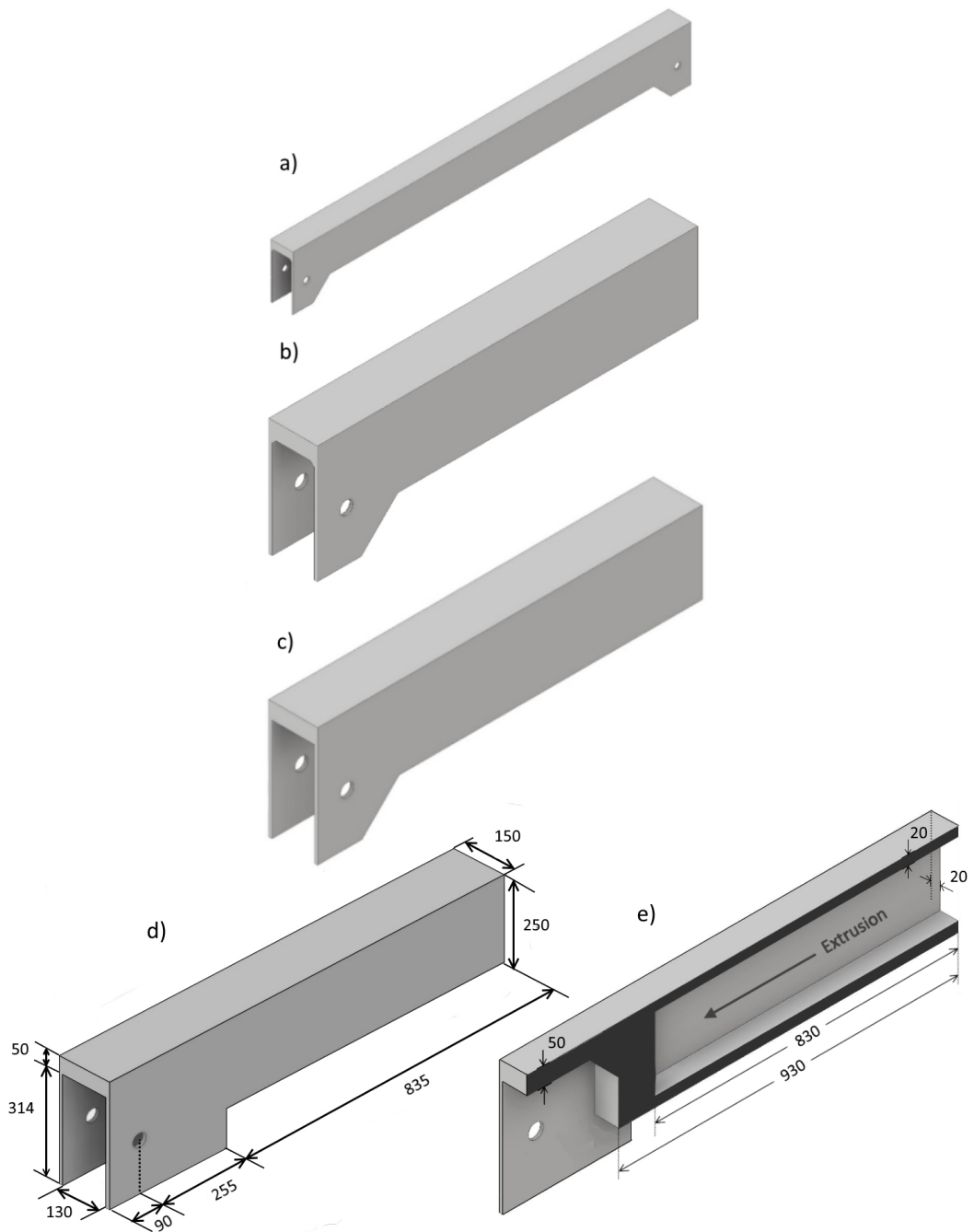
Figure 3.4: Draft of design space: a) 1st draft; b) 2nd draft, improved computational demand by exploiting symmerty; c) 3rd draft, removed chamfered edges to allow meshing with hexagon elements; d) 4th and final draft, side skirts were expanded after preliminary analysis indicated a need for more freedom in material distribution in these areas; e) Slice of model at YZ-plane.
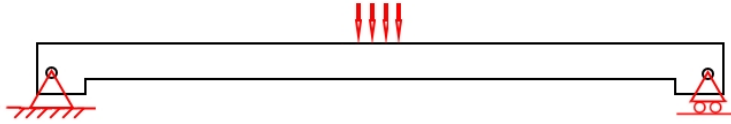
Figure 3.5: Simply supported beam, loads originating from overhead beam.
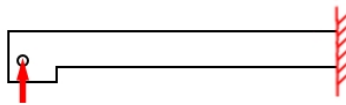
Figure 3.6: Cantilevered beam, loads originating from wheels.

design space was reduced significantly from first to second draft. There were two main reasons for this. One reason was due to how loads would be applied, which will be discussed in section 3.3.3. The other reason was to improve computation time of the analysis by reducing the number of elements created. This could easily be achieved by exploiting the symmetry of the object.

Preliminary topology optimization analysis showed that material consequently was removed round the center of the RHS part of the design space. Therefore, to further reduce computation time, material was removed from this area manually from the design space with an extrusion as seen in fig. 3.4e (this area were previously completely filled with material).

3.3.3 Loads

Two ways of applying the loads were considered. As a simply supported beam (fig. 3.5) or as a cantilevered beam (fig. 3.6) . Both cases have some advantages and disadvantages. A simply supported beam is a more accurate representation of the actual situation, with the majority of the loads originating from the overhanging hoisting beam and one could avoid using fixed support conditions which are regarded as arbitrary restrictive. However the number of elements will be twice as many as the cantilevered case. Also, the loading data provided by TKS is expressed as wheel loads, which, if the load were to be applied at the middle of the beam, would require redefining/recalculating of the loads. This work would involve approximation and assumptions which could be avoided by considering the cantilevered beam, where the loads would be defined at the wheels.

One load case was analyzed. The loads include the forces present at the wheels when the hoisting apparatus on the overhead beam is located at minimum length from the end truck considered and is hoisting maximum load. The forces are derived from TKS's standard design procedures. The load data can be viewed in appendix A.1. The load case considered consist of the loads seen

Vertical:		Horizontal:		Lateral:	
$R_{max}Dyn$	64,0 kN	K_r	1,50 kN	S	19,9 kN
		$F_{b,1}$	18,8 kN		

Table 3.1: Loads considered in analysis.
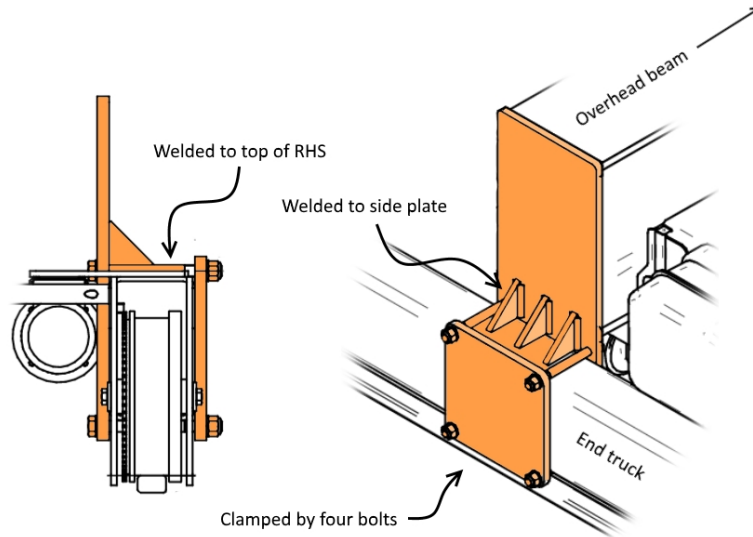
Figure 3.7: Front and isometric view of the connection between end truck and overhead beam.

in table 3.1 . The vertical, horizontal and lateral loads were according to DIN[6] 4132, DIN 15018 and FEM analysis, except the buffer force which is used for designing the crane runway end stops. To replace the buffer force, the bumper force according to AISC[7] 7 was used. The bumper force is smaller in magnitude than the buffer force because of safety factors. For the vertical load, two values where available: one from static analysis, and one from dynamic analysis. The dynamic load is slightly larger than the static load. Therefore, all though dynamic analysis would not be performed in this thesis, the dynamic load was chosen as a conservative approach. How the loads was implemented in the FEM model will be discussed in section 3.4.2.

3.3.4 Support conditions

When approximating the problem as a cantilevered beam some special considerations were taken. The connection between the larger overhead beam and the end trucks can be seen in fig. 3.7 . To make the new geometry produced by the topology optimization easier to implement into the total assembly of the overhead crane, it was deemed practical to keep this connection as is. Meaning,

---

[6]Deutsches Institut für Normung
[7]American Institute of Steel Construction
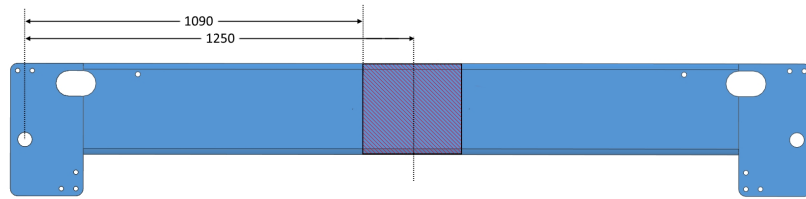
Figure 3.8: Section involved in connection (fig. 3.7) excluded from analysis.

the RHS part of this connection would be excluded from the optimization as illustrated in fig. 3.8 .

Although excluded from the optimization, the connection still had to be considered in how boundary conditions were defined. As illustrated in fig. 3.9a, a simply supported beam approach would allow the connection part to bend according to the stiffness of the beam structure. It was considered more accurate to assume that the connection would provide increased stiffness to the middle section of the beam. Simplified, the middle section would be assumed to remain straight, as illustrated in fig. 3.9b. Given how the end truck is connected to the overhead beam, with plates clamped on both sides with four bolts and welded connections at the top, a fixed connection was deemed to be a fair approximation. The problem was then viewed as a cantilevered beam with a distance from fixed support to wheel center of 1090 mm.
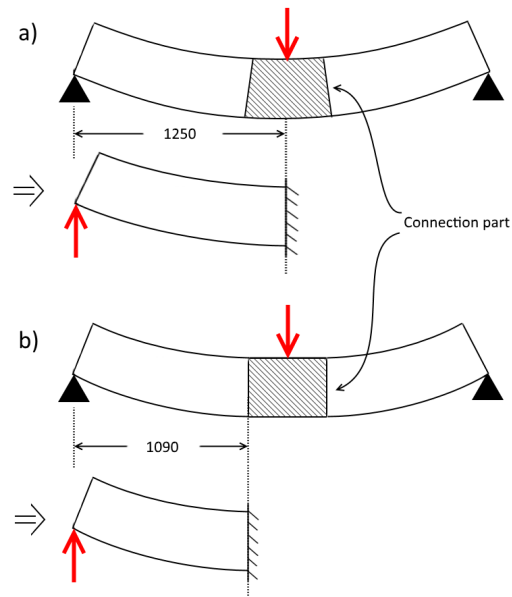
Figure 3.9: Simply supported beam redefined as a cantilevered beam: (a) with connection assumed to bend with the beam; (b) with connection assumed to provide extra stiffness (remain straight).

3.4 Implementation in Abaqus

The Abaqus CAE enviroment comprised of several modules:

- *Part* - Modeling.

- *Property* - Assigning material properties.

- *Assembly* - Assembly of parts.

- *Step* - Defines how conditions change during analysis.

- *Interaction* - Define interaction effects.

- *Load* - Defining loads and boundary conditions.

- *Mesh* - Assigning meshing parameters and element types.

- *Optimization* - Defining optimization tasks.

- *Job* - Defining analysis.

- *Visualization* - Reviewing analysis results and extracting data.

The work done in each module will not be discussed in detail. The first five modules will be discussed in section 3.4.1; loads in section 3.4.2; meshing in section 3.4.3; Optimization and job in section 3.4.4 and visualization in section 3.5.

3.4.1 3D-model

The design space was modeled in Inventor and later imported as one part in Abaqus. In the part module, several partitions were made to the model. Partitions serve two purposes. First, to define surfaces where loads can be applied (fig. 3.10a); second, to enable automatic meshing of hexahedron elements (fig. 3.10b). The material properties assign to the model was an elastic modulus of 200 GPa and a Poisson's ratio of 0,3. A standard default load step was created and used throughout every analysis. No special interaction effects were defined.

3.4.2 Loads and supports

Loads where applied as pressure loads. Using Newton and millimeter as units, pressure loads are stated as N/mm^2(MPa). The loads shown in table 3.1 were implemented the following way.

3.4.2.1 Vertical and horizontal loads

The vertical and horizontal loads were implemented in equal fashion, over equal amount of area. Vertical load was applied at surface shown in fig. 3.13a, while horizontal loads were applied at surface shown in fig. 3.13b. The loads were halved and applied at both wheel-holes. In Abaqus, the default distribution of pressure loads are uniform and normal to the surface. Using this distribution would be an inaccurate representation of how the load would act on the hole-surface (fig. 3.11a) . To better represent a bearing load type (fig. 3.11b), an
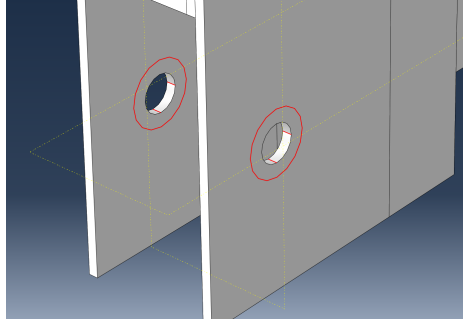
(a) For load defining purposes.
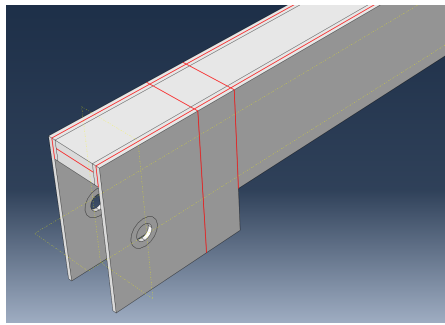
(b) For hexahedron element meshing purposes.

Figure 3.10: Partitions (marked in red).
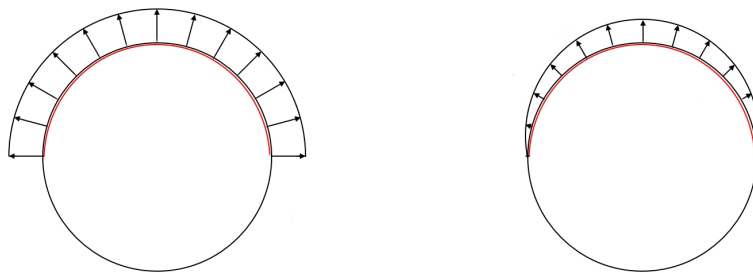
(a) Default pressure load distribution in Abaqus.

(b) Sinusodial bearing load distribution.

Figure 3.11: Load distribution.
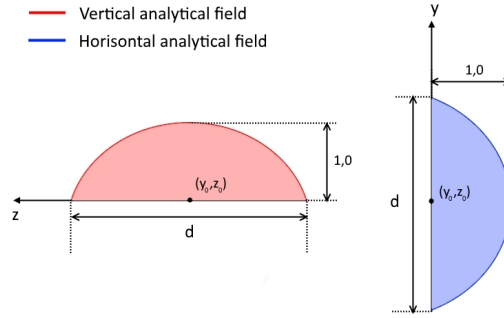
Figure 3.12: Analytical fields.

Algorithm 3.1 From point load to bearing load.

1. Divide P on each wheel hole: $\dfrac{P}{2} = P'$.

2. From point load P' to line load w: $\dfrac{P'}{10} = w$,

   where 10 is the thickness of the plate in mm.

3. From line load w to pressure load q: $\dfrac{w}{a} = q$,

   where $a = r \displaystyle\int_{-\frac{1}{2}\pi}^{\frac{1}{2}\pi} \cos\left(\theta\right) d\theta$.

Analytical Field was created and assign to the distribution control. Analytical Field is a tool in Abaqus for creating mathematical expressions. Two Analytical Field was defined (illustration can be seen in fig. 3.12) :

$$\text{For vertical loads:} \quad f\left(z\right) = \cos\left(\pi \frac{\left(z_0 - \mid z \mid\right)}{d}\right) , \tag{3.1}$$

$$\text{for horisontal loads:} \quad f\left(y\right) = \cos\left(\pi \frac{\left(y_0 - \mid y \mid\right)}{d}\right) . \tag{3.2}$$

Where y_0 and z_0 are coordinates for the center of wheel holes (true for both holes), and d is the diameter of wheel hole (40 mm).

The loads given in table 3.1 had to be redefined as bearing loads. To determine the magnitude of the vertical and and horizontal bearing load, the area of the applied surface and the analytical fields had to be considered. The surface area have width of 10 mm and a length of : $\pi \times r$, where r is the radius of wheel hole (20 mm). The loads (P) were transformed to pressure loads with algorithm 3.1. The value a in algorithm 3.1 reflect the surface length and the analytical fields seen in eq. 3.1 and 3.2 . The redefined loads can be seen in table 3.2.

Name	P [N]	P' [N]	w [N/mm]	q [N/mm^2]
R_{max}Dyn	64 000	32 000	3200	80
K_r	1500	750	75	1,88
$F_{b,1}$	18 800	9400	940	23,5

Table 3.2: Redefined loads from table 3.1.

3.4.2.2 Lateral load

The were some uncertainty in how the lateral load should be applied to best represent actual loading behavior. The approach presented here was done by intuition by the author. The lateral load was applied on the surface shown in fig. 3.13c as a uniformly distributed pressure load amounting to a total force of 9950 N per wheel hole. The surface area is defined by the circumference of the wheel hole and a larger circle with a radius of 35 mm.

3.4.2.3 Support

The support was defined at the surface shown in fig. 3.13d. Displacement in x, y and z direction was fully restricted. Rotational restriction was not necessary because of the elements used in analysis, which will be discussed in the next section.

3.4.3 Meshing

Two methods of meshing the model were available, with hexahedron elements (six faces) or tetrahedron elements (4 faces). In Abaqus, the tetrahedron meshing algorithm is more flexible than the hexahedron meshing, which might (and did in this case) require partitioning. Meshing greatly influence the computational time for standard analysis. Especially when preforming a topology optimization analysis with SIMP, where a static analysis is performed after every iteration. For this model, topology optimization converged at about 50 iterations. Meaning, a topology optimization would take at least 50 times longer than a standard static analysis (not including the time of the topology optimization routine of each iteration). Therefore, meshing should be given special consideration.

In addition to the computation time consideration, there is a competing factor relating to the preferred geometrical detail of the end topology to utilize the capabilities of a 3D-printer. Because of the relative large difference between dimensions of the design space (over 1 m in length) and the level of detail a 3D-printer provides, it was a challenge to develop a mesh which provided sufficient geometrical detail, while simultaneously keep the computational demand satisfactory low.

Computational demand depend mainly on element type and fineness of mesh. Element types considered were linear hexahedron elements, quadratic hexahedron elements and quadratic tetrahedron elements (fig. 3.14) . Quadratic elements would be preferred for better accuracy. Fineness of mesh in Abaqus is controlled by "seeding". Seeding is specified at edges of the model by either a physical size which the elements should approximate, or by determining the

(a) Vertical load.

(b) Horizontal load.

(c) Lateral load.

(d) Boundary condition.
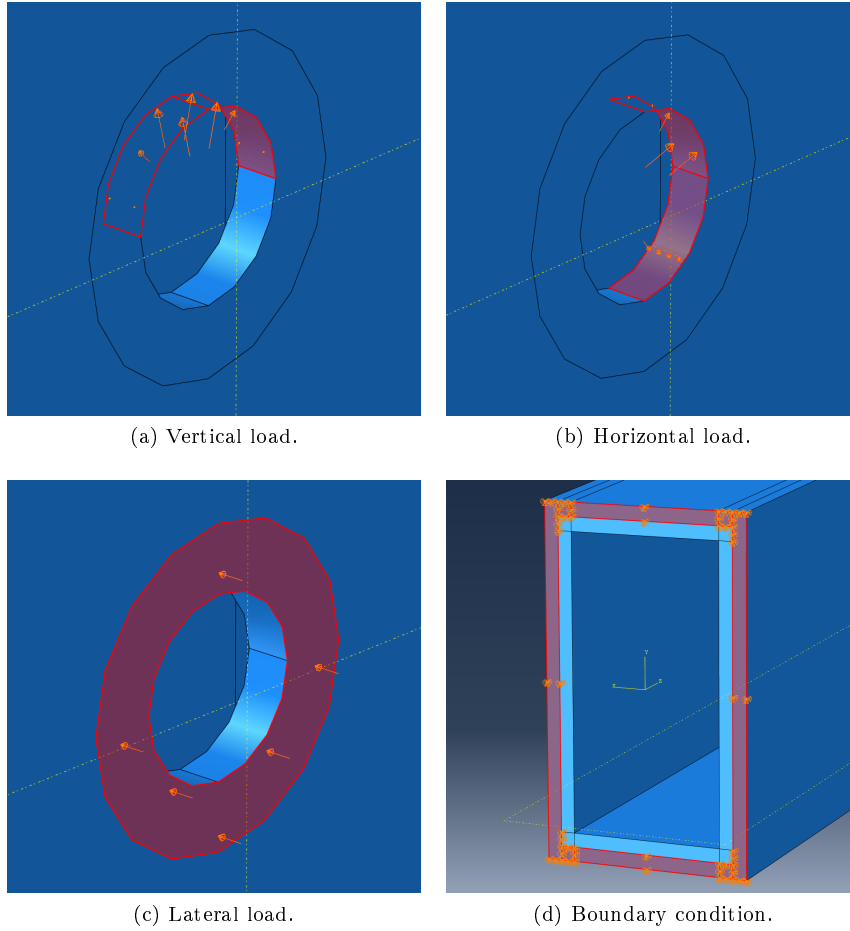
Figure 3.13: Surfaces in FE model for loads and boundary conditions.
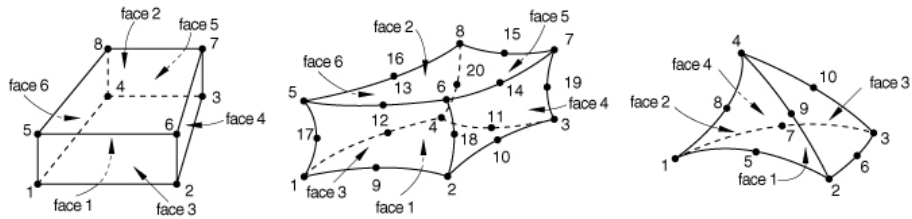
Figure 3.14: Elements. From the left: 8-node linear hexahedron; 20-node quadratic hexahedron; 10-node quadratic tetrahedron.[44]
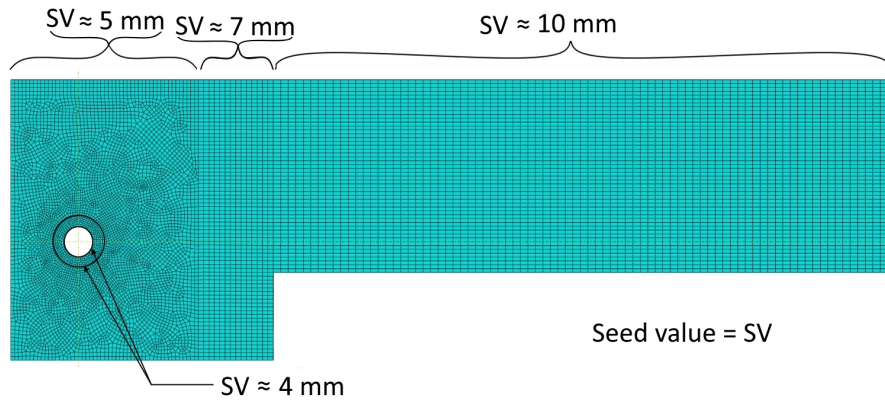
Figure 3.15: Seed values applied at edges to controll mesh element sizes.

Type	No. of nodes	Time static	Est. time of topology optimization
Tetrahedron	893 986	9 min 25 sec	≈ 9 h
Quad. hexahedr.	506 386	5 min 20 sec	≈ 6 h
Lin. hexahedr.	133 100	40 sec	≈ 50 min

Table 3.3: Comparison of element types.

number of mesh elements directly. The minimum member size of WAAM components were used as a guideline for detail level in the mesh. [19] report a typical minimum feature size for a WAAM process to be 2 mm. A global seeding of approximately 5 mm were chosen with some local variations illustrated in fig. 3.15. The level of fineness in the mesh was slightly reduced towards the support end, prioritizing a more detailed mesh at the wheel holes.

The computation time of the different elements previously mentioned was compared by doing a standard static analysis. Table 3.3 present the results. There was a problem of artificially high stress values at the sharp edges of the model for both quadratic element types. Mesh refinement and softening edges were attempted to improve this, but was not achieved without increasing analysis time to an unacceptable degree. Meshing with tetrahedron elements also produced distorted elements, which should be avoided. Because of this and the relatively large difference in computation time, linear hexahedron element type was chosen. The final mesh had 107 306 elements.

3.4.4 Setup of topology optimization

Abaqus have a build in optimization routine for topology optimization, which different controllers attached to it. This section will present how these controllers were set up. The topology optimization controllers in Abaqus consist of: Design response, Objective functions, Constraints, Geometric constraints and Stop conditions. In addition to these controllers, there are some general parameters which will be discussed in section 3.4.4.1. A total of five optimization
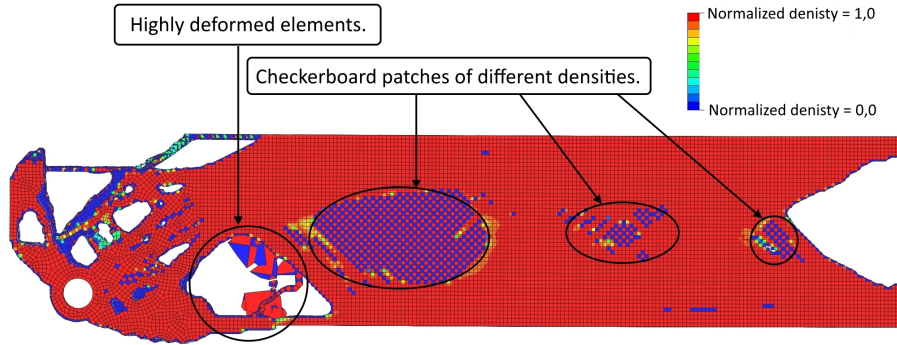
Figure 3.16: Problems with initial topology optimization runs (side view).

task were defined, differentiated only by different volume fraction constraints (discussed in 3.4.4.4). This approach of studying different volume fractions was largely inspired by the work of [45].

3.4.4.1 General parameters

Mainly default values were kept. Load regions were frozen, meaning surfaces where loads had been applied would not be changed, surfaces where boundary conditions were defined were not frozen.

The parameters for the convergence criteria turned out to be quite critical for successful topology optimization. Initially the default parameters were chosen: *objective function delta criterion* = 0,001 and *element density delta criterion* = 0,005. Tosca documentation define these criteria:

$$\frac{|\Theta_n - \Theta_{n-1}|}{|\Theta_n|} \leq \text{objective function delta criterion.}$$

Where Θ_n is the objective variable value of current iteration and Θ_{n-1} the value of previous iteration.

$$\frac{\displaystyle\sum_1^{\text{Number of elements}} |\rho_n - \rho_{n-1}|}{\text{Number of elements}} \leq \text{element density delta criterion.}$$

Where ρ_n is the density of a element of current iteration and ρ_{n-1} the density of a element of previous iteration. Initial optimization runs with default settings showed unclear topology with unintuitive features (fig. 3.16)[8] . Investigating this issue showed that lowering the value of the convergence criteria improved results. The convergence parameters were set to: *objective function delta criterion* = 0,0004 and *element density delta criterion* = 0,004.

Equal for all optimization task were a SIMP penalty factor $p = 3,5$ after recommendation from [10] stating that a penalty factor of $p \geq 3$ is often required for obtaining clear "0-1"-topologies (as discussed in section 2.2.3.2).

---

[8]Checkerboard problem shown in fig. 3.16 is not to be confused with the checkerboard problem discussed in section 2.2.3.3. Abaqus/Tosca have filters that prevent the formation of checkerboard patterns in the way it is presented in 2.2.3.3. [44]

3.4.4.2 Design response

Two design responses were defined, namely strain energy and volume. Strain energy will be the objective variable while volume will be the constraint variable.

3.4.4.3 Objective function

The objective function was decided to be a minimum compliance problem, or maximum stiffness, as discussed in section 2.2.3.1. To find maximum stiffness, the strain energy will be minimized. In Abaqus there were two relevant objective functions; minimize design response or minimize the maximum design response (often referred to as min-max formulation[44]). Abaqus documentation explain the two different formulations in the following way:

> Minimize design response values: create an optimized model that tries to minimize the sum of the weighted differences between the design response and the reference value. [44]

> Minimize the maximum design response values: find the maximum weighted difference between the design response and the reference value and create an optimized model that minimizes that maximum difference. [44]

Tosca documentation [44] gives a more detailed insight into the mathematical differences (in compliance terms):

$$\text{minimization:} \quad \min(+\alpha C_k)\,,$$
$$\text{minmax:} \quad \min(|\alpha(C_k - C_k^*)|)\,.$$

Where α is weight factor and C_k is compliance and C_k^* is a compliance reference value normally set to 0. This min-max formulation is similar to *the bound formulation* presented in [46], which states that the bound formulation is used to optimize the worst possible case of multiple load cases. Although multiple load cases was not defined in this thesis, the min-max formulation was used because of it's higher flexibility in a general sense compared to the minimize formulation.

3.4.4.4 Constraints

Without a constraint on the objective function, the design space would remain unchanged after analysis and nothing would be accomplished. The objective function would be constraint by the amount of volume used relative to the starting design space volume. The goal was to find the lowest volume fraction constraint that would still produce a topology which satisfies a yielding criteria. The volume fraction were determined by considering percent reduction from the volume of the original beam structure seen in fig. 3.3, from 0% reduction to 40% reduction with increments of 10%. The volume of the original beam structure relative to the design space is 0,346. A topology optimization analysis was performed for each volume reduction increment and the fractions can be seen in table 3.4, and every volume constraint was defined as a less or equal constraint.

Analysis name	Volume reduction	Fraction of original part	Fraction of design space
topo_opt_100	0 %	1,0	0,346
topo_opt_090	10 %	0,9	0,312
topo_opt_080	20 %	0,8	0,277
topo_opt_070	30 %	0,7	0,242
topo_opt_060	40 %	0,6	0,208

Table 3.4: Volume fractions used as constrains in topology optimization.
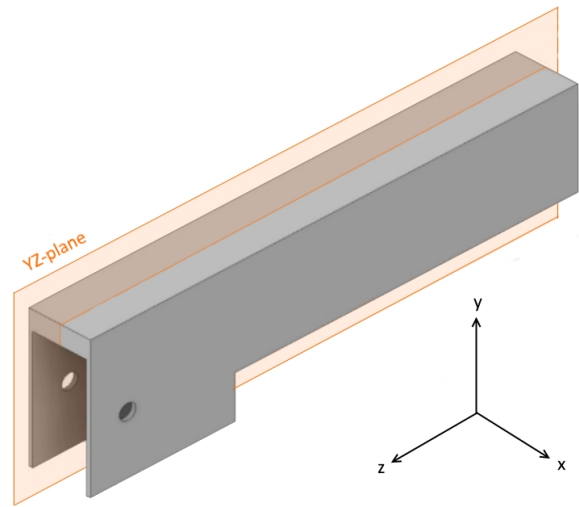
Figure 3.17: Symmetry plane.

3.4.4.5 Geometric constrains

Geometric constraints are not related to design variables and include restrictions like symmetry, minimum member size, maximum member size, etc. A symmetry restriction was implemented on the YZ-plane (illustrated in fig. 3.17). This was mainly due to the lateral loads, which could be applied in either direction. The symmetry requirement would result in a topology which could withstand the lateral loads in both directions.

3.4.4.6 Stop conditions

A maximum number of iterations were set to 70 to prevent non-convergent optimizations to run endlessly, otherwise the optimizations would stop when the convergence criteria mentioned in section 3.4.4 were satisfied.

3.5 Results

Result of the five topology optimizations will be presented in this section.

3.5.1 Iteration data

Values of the design variables are stored for each iteration. These data can be view in appendix B.1. The data was plotted on a graph to illustrate the convergence process and can be viewed in fig. 3.18-3.22. The figures show a stable convergence of strain energy for all analysis. Volume display a more jagged convergence, but in similar fashion for all analysis.

3.5.2 Topologies

The topologies can be seen in fig. 3.23-3.27. The output variable of topology optimization in Abaqus is a *Material Property Normalized* (MPN) variable equal in purpose to the density variableρ discussed in section 2.2.3.2, eq. 2.2 . The topologies are visualized by creating a view cut which use the MPN variable to only show elements with a value larger than some value between 0 and 1 (referred to as isosurface value (ISO) in abaqus). The default ISO value is 0,3 , meaning every element with a MPN value of less than 0,3 will be hidden. This setting seemed to produce a clear, continuous geometry, so the ISO value of 0,3 was not changed.

Outer boundaries of the final geometries appear near equal in all cases, with internal boundaries being the differentiating feature. Bendsøe and Sigmund [10] mentions that topologies produced from SIMP-optimization routines with a low fraction of available volume relative to volume of design space tends toward a truss-like structure. This tendency can be observed, especially for the 30% and 40% volume reduction topologies.

3.5.3 Yield criterion

To determine which topology to use as a basis for further design, the general elastic yield criterion given in NS-EN 1993-1-1:2005 (Eurocode 3) clause 6.2.1 was used. In this clause, it states that the yield criterion shall be considered at a critical point in a cross section. The topologies obtained after analysis have a varying cross section. Therefore, point of maximum Von Mises stress were used as a guideline to determine location of the critical point. For all topologies, maximum Von Mises stress were located at point seen in fig. 3.28. Stress data were extracted from a path as seen in fig. 3.29. Normal stress, transverse stress and shear stress values were extracted from the path and used in the yield check specified in Eurocode 3 eq. 6.1:

$$\left(\frac{\sigma_{x,Ed}}{f_y/\gamma_{M0}}\right)^2 + \left(\frac{\sigma_{z,Ed}}{f_y/\gamma_{M0}}\right)^2 - \left(\frac{\sigma_{x,Ed}}{f_y/\gamma_{M0}}\right)\left(\frac{\sigma_{z,Ed}}{f_y/\gamma_{M0}}\right) + 3\left(\frac{\tau_{Ed}}{f_y/\gamma_{M0}}\right)^2 \leq 1 \quad (3.3)$$

where $\sigma_{x,Ed}$ is the normal stress; $\sigma_{z,Ed}$ is the transverse stress; τ_{Ed} is the shear stress; f_y is yield strength of steel and γ_{M0} is the material safety factor. Steel type considered were S355 with $f_y = 355\,MPa$ and $\gamma_{M0} = 1,05$ (according to National Appendix of Eurocode 3). The coordinate system in the FE-model is oriented differently than what is given in the standard. In the FE-model, normal stress would be the z-axis (designated as S33 in Abaqus); transverse stress is along the x-axis (S11) and the shear stress is parallel to the XY-plane (S12). Fig 3.30 shows the data and the yield criterion check for each topology. From fig. 3.30 it is seen that the "*topo_opt_070*" topology (30% volume reduction) failed
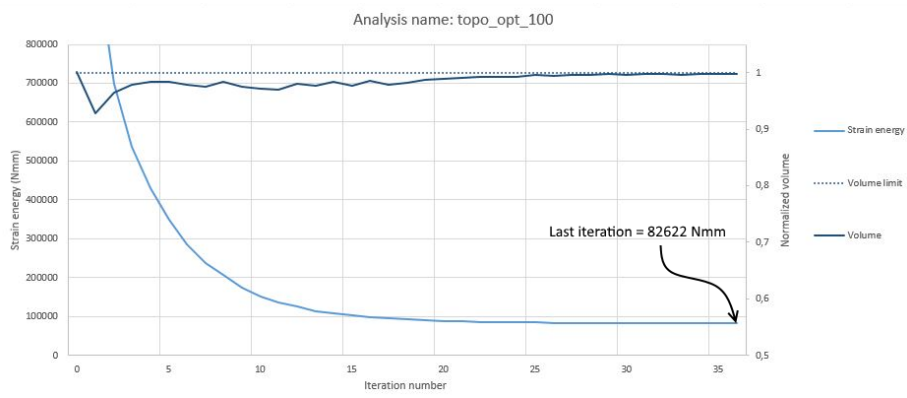
Figure 3.18: Convergence of design variables (0 % volume reduction).
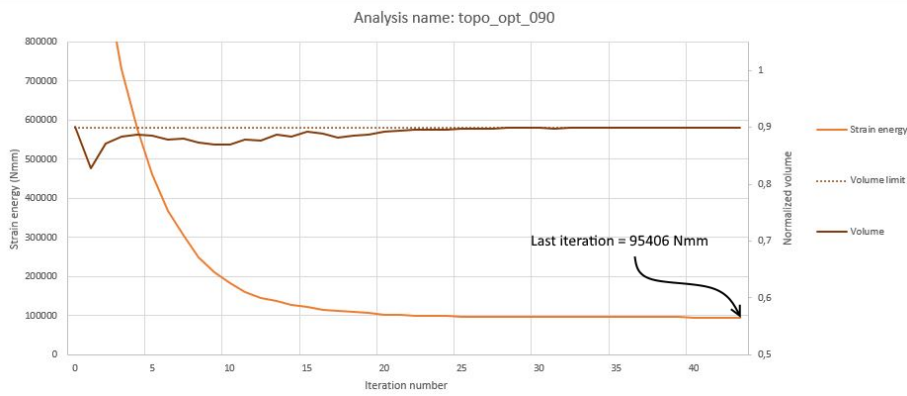
Figure 3.19: Convergence of design variables (10 % volume reduction).
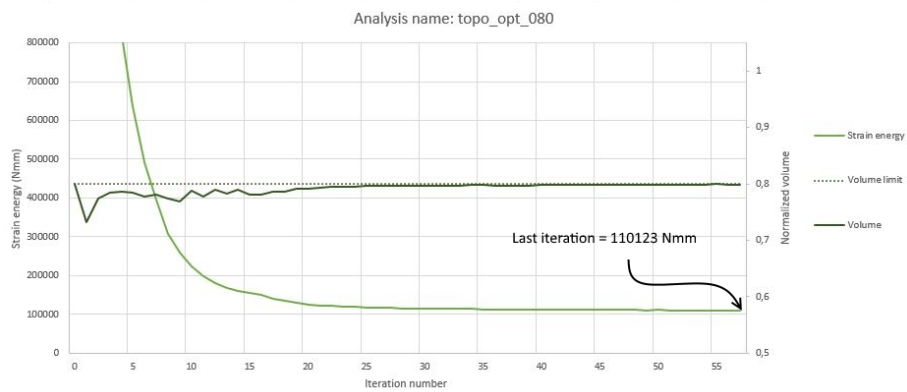
Figure 3.20: Convergence of design variables (20 % volume reduction).
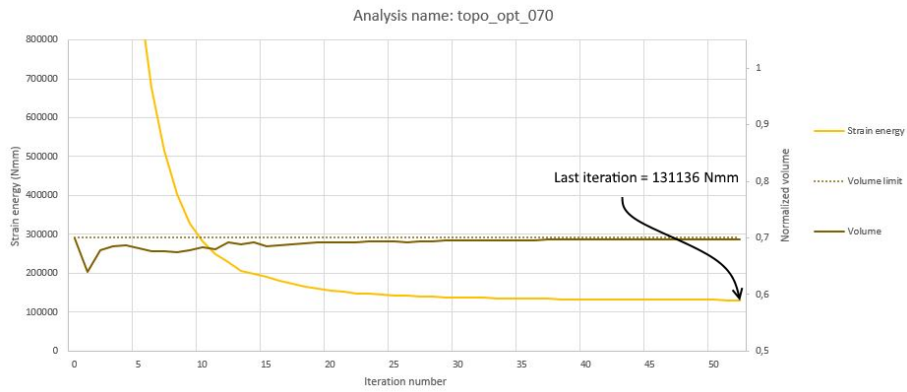
Figure 3.21: Convergence of design variables (30 % volume reduction).
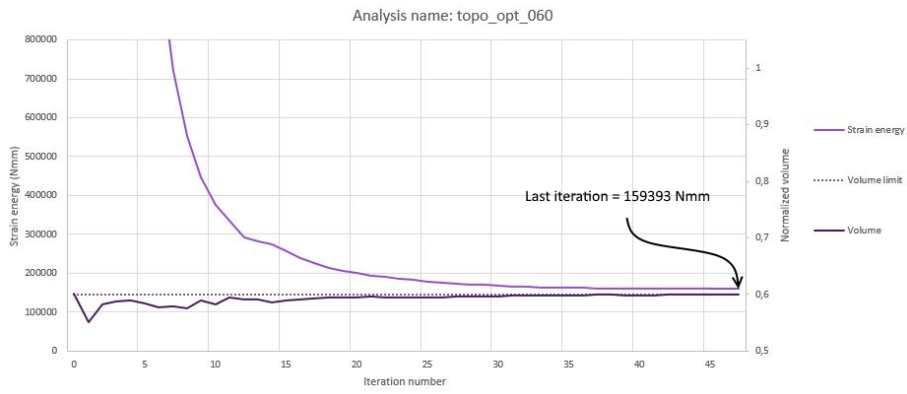
Figure 3.22: Convergence of design variables (40 % volume reduction).
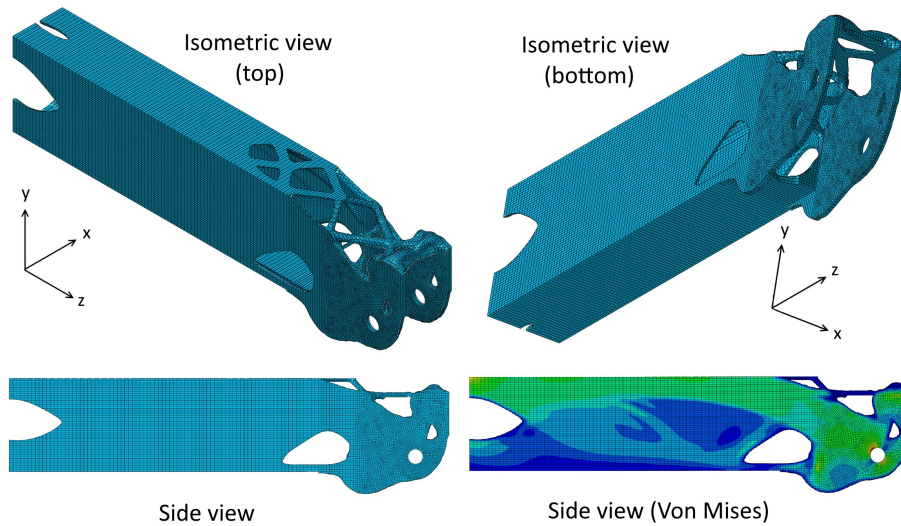
Figure 3.23: "topo_opt_100" (0% volume reduction).
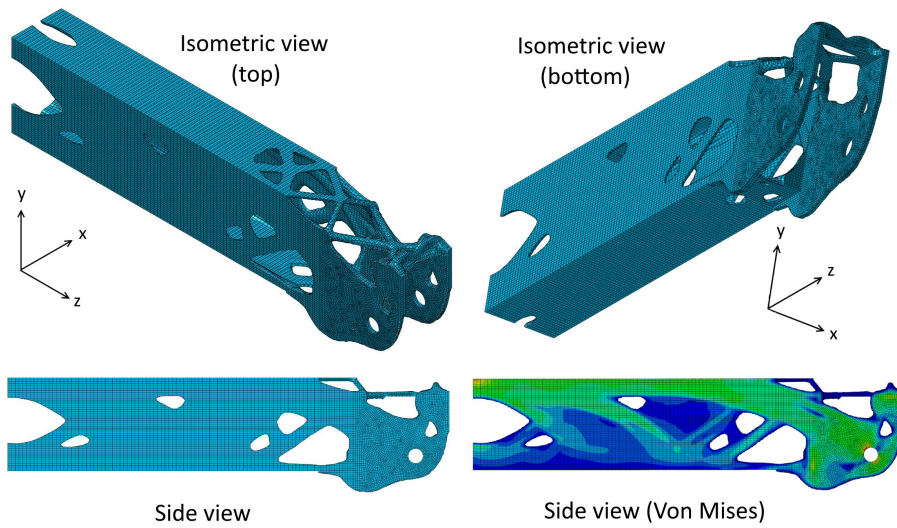
Figure 3.24: "topo_opt_090" (10% volume reduction).
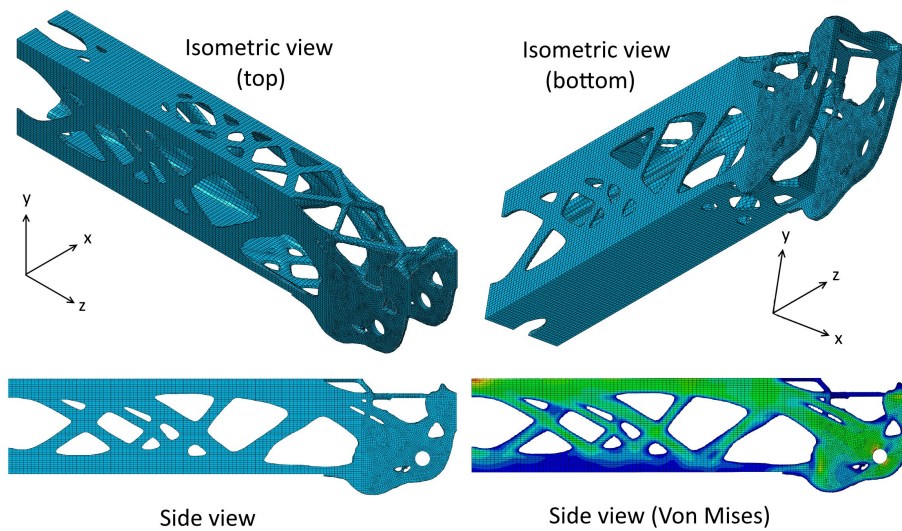
Figure 3.25: "topo_opt_080" (20% volume reduction).
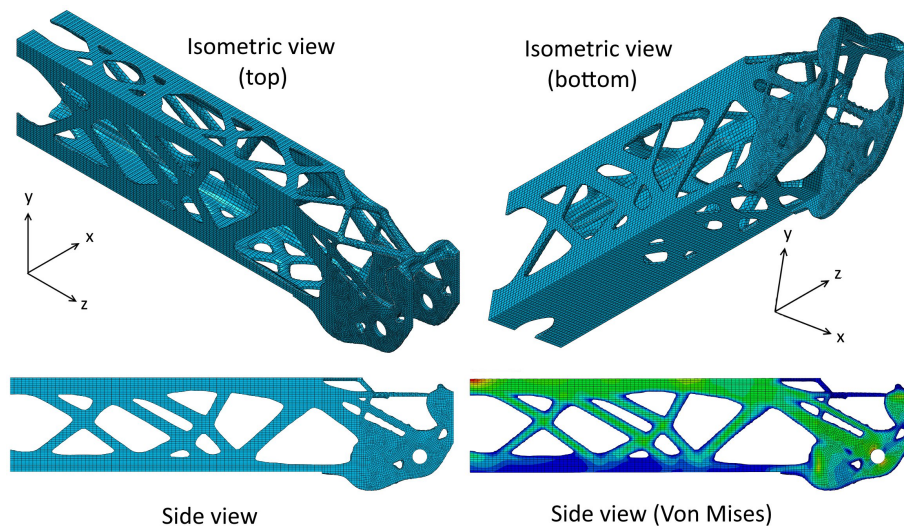
Figure 3.26: "topo_opt_070" (30% volume reduction).
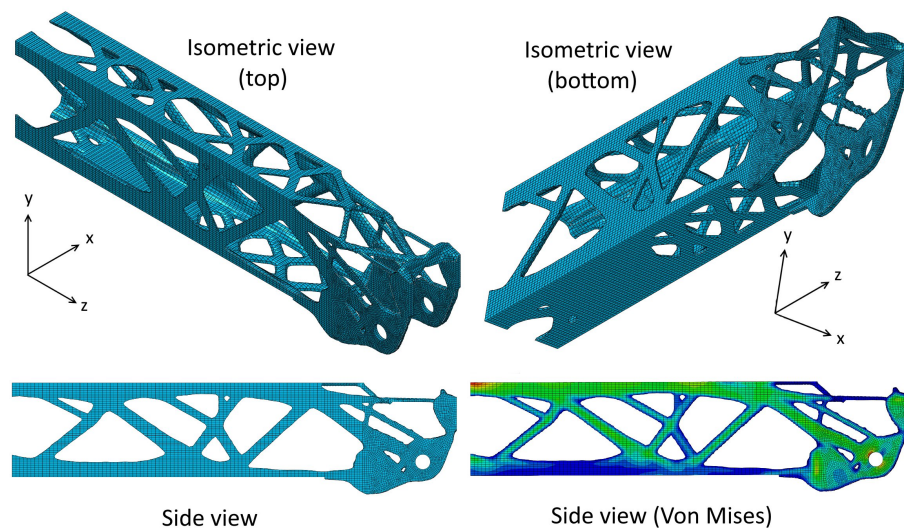
Figure 3.27: "topo_opt_060" (40% volume reduction).
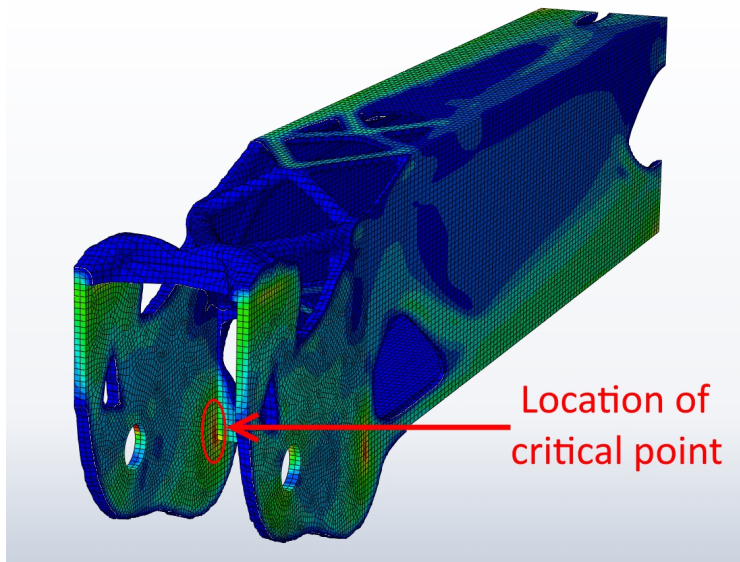
Figure 3.28: Location of critical point.
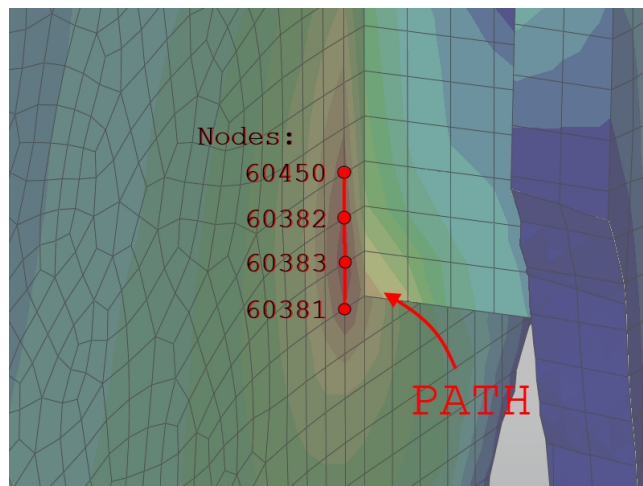
Figure 3.29: Path containing four nodes at critical point.

the yield check, making "*topo_ opt_ 080*" (20% volume reduction) the topology
to be considered as a guideline for design.

Critical point yield check:

Yield stress (MPa)
355

topo_opt_100:

Node	Normal (MPa)	Transverse (MPa)	Shear (MPa)	Eq. 6.1 (Eurocode 3)
60450	274,29	8,18	−9,58	0,64
60382	290,55	9,97	−4,99	0,71
60383	296,19	13,61	6,44	0,73
60381	268,57	9,57	19,27	0,62

topo_opt_090:

Node	Normal (MPa)	Transverse (MPa)	Shear (MPa)	Eq. 6.1 (Eurocode 3)
60450	297,44	9,00	−8,10	0,75
60382	311,55	10,55	−3,26	0,82
60383	314,30	13,74	8,43	0,83
60381	282,88	9,22	20,90	0,69

topo_opt_080:

Node	Normal (MPa)	Transverse (MPa)	Shear (MPa)	Eq. 6.1 (Eurocode 3)
60450	316,90	9,56	−8,41	0,85
60382	330,90	11,25	−3,13	0,93
60383	332,54	14,70	9,41	0,93
60381	298,11	9,81	22,50	0,77

topo_opt_070:

Node	Normal (MPa)	Transverse (MPa)	Shear (MPa)	Eq. 6.1 (Eurocode 3)
60450	347,89	10,30	−9,07	1,03
60382	363,26	12,39	−2,86	1,12
60383	364,67	16,21	10,92	1,12
60381	327,18	10,72	24,82	0,92

topo_opt_060:

Node	Normal (MPa)	Transverse (MPa)	Shear (MPa)	Eq. 6.1 (Eurocode 3)
60450	391,44	11,97	−11,19	1,30
60382	409,31	14,08	−3,19	1,42
60383	412,29	18,40	12,48	1,43
60381	370,84	12,10	28,06	1,19

Figure 3.30: Yield criteria check.

44

3.6 Post-processing of optimization output

Post-processing, in this case, means the remodeling of the optimization output (topology) in Inventor and the subsequent FE-analysis of these re-imagined models in Abaqus. The aim is to provide conceptual designs on how geometry obtained from topology optimization could be realized in manufacturing, either by traditional means of by additive manufacture.

3.6.1 Extracting geometry

To obtain a computer file of the 3D-geometry of a topology optimization for further use, Abaqus has an "extract" functionality within the job module. One can either extract an Abaqus input file for further use in Abaqus, or extract a STL-file. The appearance of the exported geometry depend on several inputs, most importantly; at which iteration step in the optimization process the geometry will be extracted from and what ISO-value to be used (discussed in 3.5.2). The last iteration of optimization was used along with an ISO-value of 0,3. In addition to these choices, some additional processing alternatives are available, like reduction and smoothing of surfaces. Smoothing had quite a large effect on one particular feature of the exported geometry, shown in fig. 3.31 (discussed further in section 3.6.3), but overall improved surface finish. Default value of five smoothing cycles were chosen. Different values of percent face reduction showed little to no noticeable changes in the exported geometry and a value of 0 % was used. The geometry exported as a STL-file can be seen in fig. 3.32.

One thing to note about the exported STL-geometry is that, it might not represent a exact 20% volume reduction. All intermediate normalized densities in the output geometry will be made either 0 or 1 (depending on the ISO value). With a ISO value of 0,3 , as was used in this case, quite a large fraction of the intermediate densities would be assigned a value of 1 and would result in a increase in volume from the original geometry containing intermediate densities. A decrease in volume reduction was observed for final model of both designs.

3.6.2 Traditionally manufacture design

The design aimed for traditional manufacture (sometimes referred to as "the traditional design" in this thesis) was created from scratch in Inventor, but using
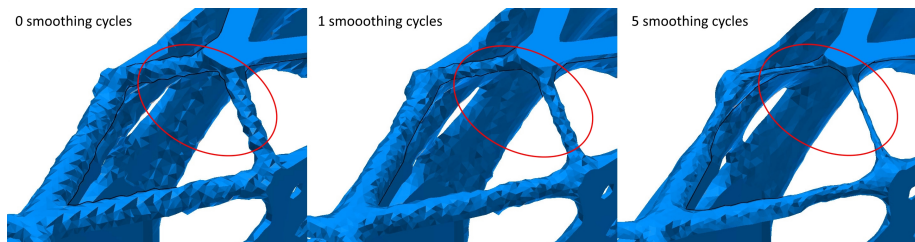
Figure 3.31: Exported geometry using different number of smoothing cycles (thinning of member marked in red). From the left: No smoothing; one cycle; five cycles.
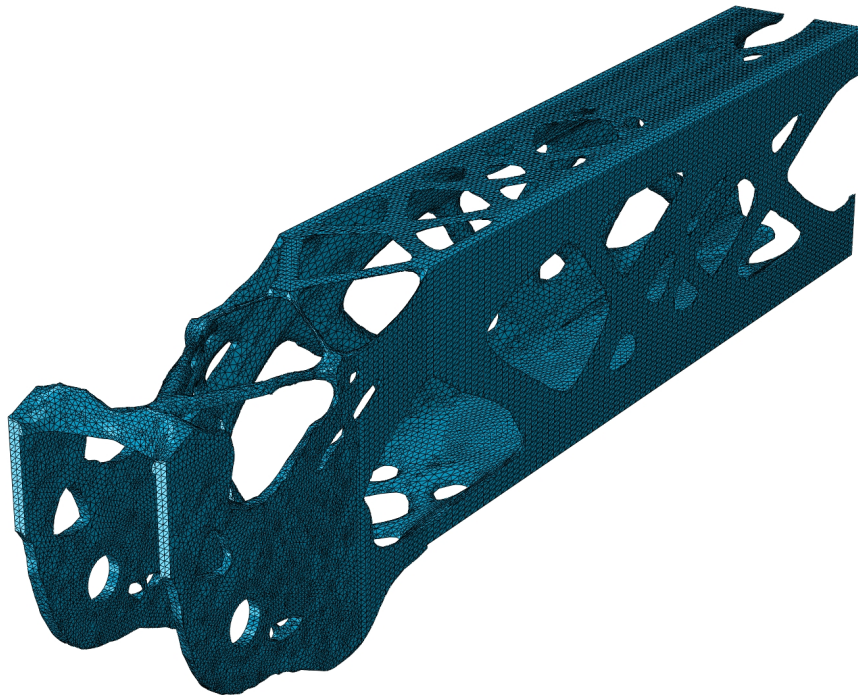
Figure 3.32: Extracted geometry in STL file format.

the STL-geometry as a guide. Features from the STL-geometry were approximated intuitively by the author, with a general goal of keeping the topology unchanged (same amount of holes) and hole dimension near equal to that of the STL-geometry.

First, the main body of the component was created by extruding a profile similar to a RHS. Then, the features from the original topology were replicated by mostly using circles, straight lines, and occasionally tangent arcs, to create the profile of outer and inner boundaries (example shown in fig. 3.33) . The holes were then cut out by using the extrusion functionality. When equal topology was achieved, most of the sharp edges were rounded-off with the fillet function. The final model can be viewed in fig. 3.34 and fig. 3.35a shows a suggestion on
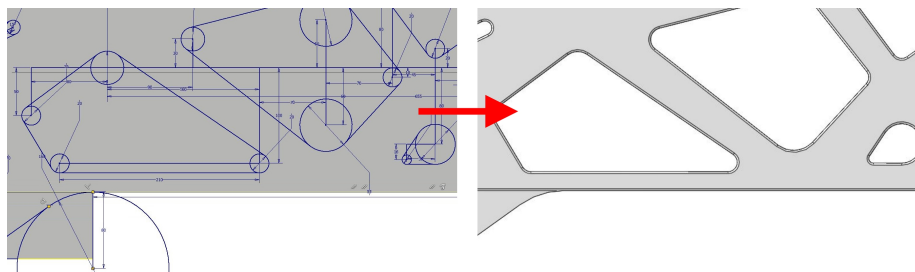
Figure 3.33: Example of how topology was created from scratch in Inventor.
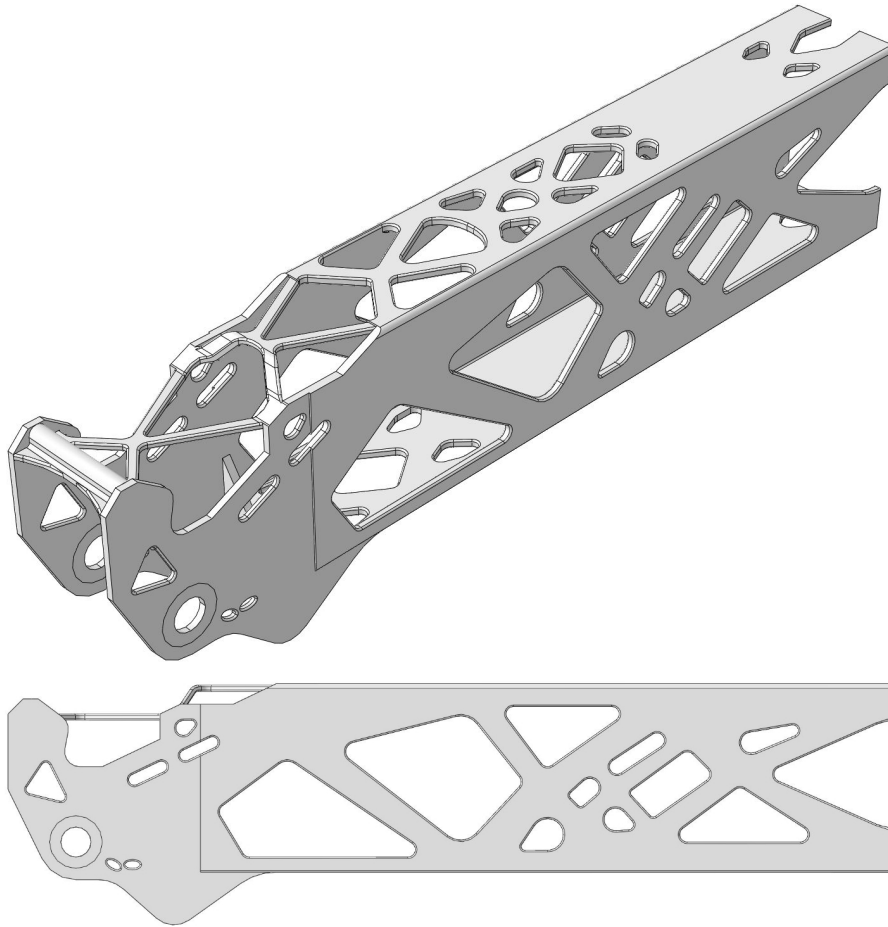
Figure 3.34: Design intended for traditional manufacturing approximating geometry from topology optimization.

how the component could be made as an assembly. Welds were not modeled, but suggestion on weld types can be seen in fig. 3.35b. The volume of the final model was the equivalent of a 17% volume reduction.

3.6.3 Additive manufacture design

When designing for additive manufacturing, the intention was to keep the geometry from the STL-file unchanged. In-fact, the original purpose of the STL file format was to represent 3D geometry in a way that could be directly interpreted by stereolithographic 3D printers [47]. However, due to the rather thin member created by the smoothing algorithm of the STL extraction in Abaqus (as seen in fig 3.31), it was deemed reasonable to remodel this feature.

The STL-format proved difficult to work with in this regard. Finding a CAD software that could edit the STL-format directly was not possible for

(a) Suggestion on assembly.   (b) Suggestion on welding.
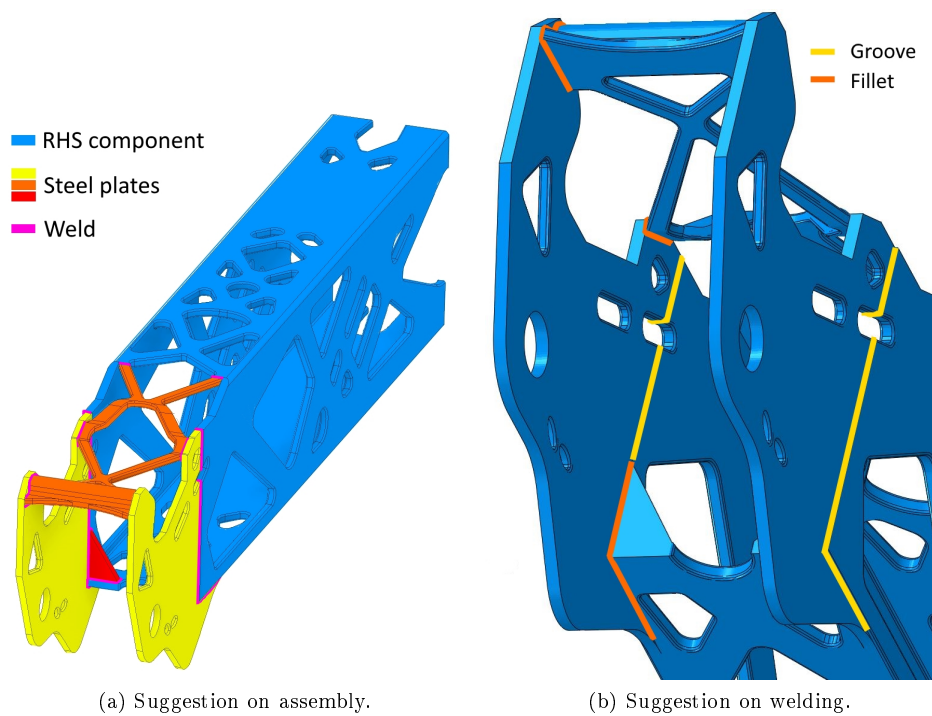
Figure 3.35: Manufacturing suggestions.

the author. To obtain an editable 3D-model, an Inventor add-in[9] called Mesh Enabler[10] was used. Mesh Enabler could transform the STL-geometry to a workable format. No topological differences in the geometry were observed after the transformation. The geometry could then be edited with Inventor.

Three changes were made to the geometry obtained from the STL-file. The first were the member seen in fig. 3.31. This member was remodeled to be slightly thicker, more equal to how the member appeared before the smoothing. The second change was the removal of a particular sharp edge, seen in fig. 3.36. The third change was a round-off of sharp corners present of the outer edges of the model. Otherwise the geometry were left unchanged. The final model can be viewed in fig. 3.37. The volume of the final model was the equivalent of a 14% volume reduction.

---

[9]Add-ins are smaller programs developed by Autodesk, or third-party developers, that offer additional functionality to the core program.

[10]Mesh Enabler is developed by Autodesk.
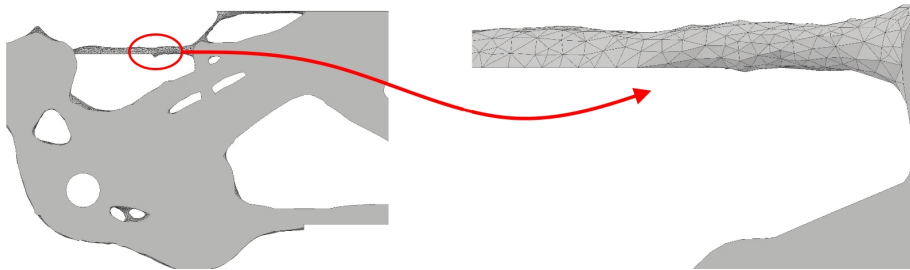
Figure 3.36: Removal of sharp edge.

a)

b)
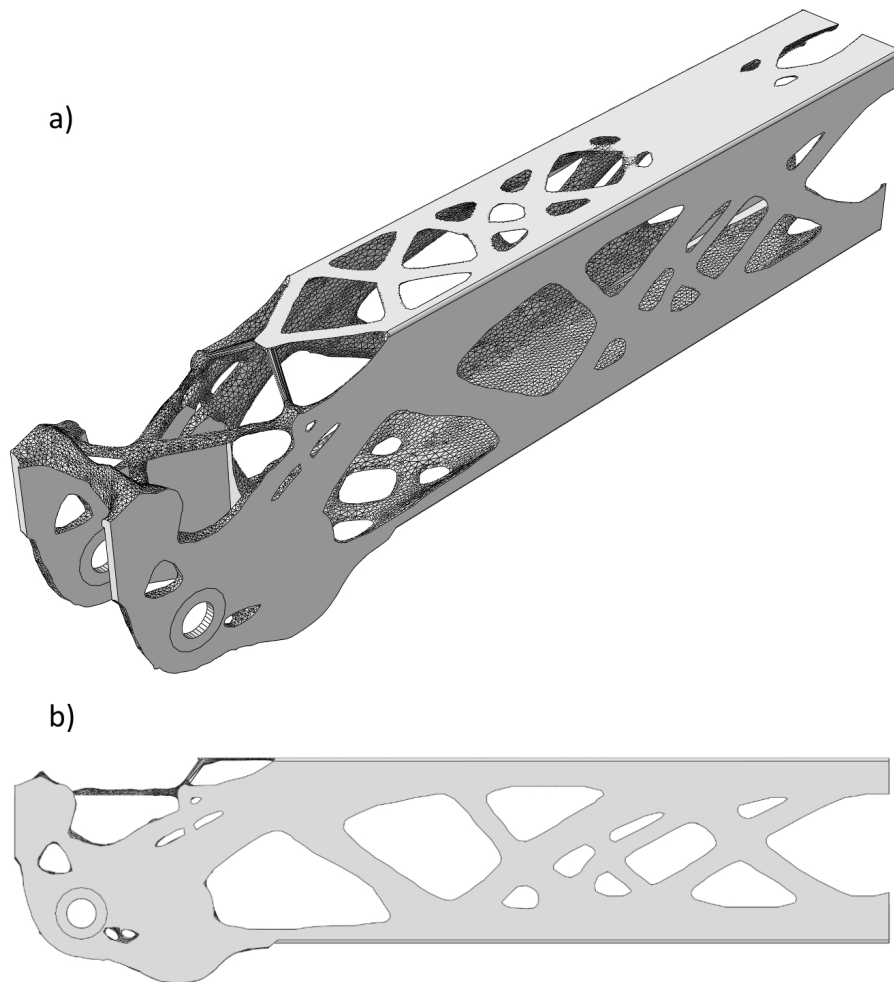
Figure 3.37: Design intended for additive manufacturing equal to geometry from topology optimization (apart from small changes mentioned in section 3.6.3).

3.7 Validating FE-analysis

As a last step, the final models created in section 3.6 were imported into Abaqus and a standard static analysis was performed as a basic validation step for the two models. Both models consisted of one solid geometry (no assembly of different parts). The exact same loads and boundary conditions were used as with the topology optimization analyses. The results are presented below. Because of the complexity in shape of both models, only tetrahedron meshing was viable. A global meshing seed of 3 mm was used (meshing algorithm will approximate an element size of 3 mm).

3.7.1 Analysis of traditionally manufacture design

Values of Von Mises stress was investigated. Several areas showed stress values above the design yield strenght of $355/1,05 = 338$ MPa. A maximum value of 1128 MPa was observed at location shown in fig. 3.38. This was located at sharp edge and the max value was most likely a singularity, but still a cause for concern.

To study the stresses in this area further, the mesh was refined at this area and resubmitted for analysis. Original seed at corner edges were 3 mm. Two new refined meshes were created with corner edge seed of 2 mm and 1 mm , seen in fig. 3.39. Fig. 3.39 also show the path of which stress values were extracted to study the stresses at sharp corner (marked in red). The data was plotted in a graph seen in fig. 3.40. Although peak values can be ignored, it is still estimated that the stress value at corner lie beyond yield strength of S355 steel.

An upper limit to the contour plot of Von Mises stress was set to 338 MPa to visualize areas were stress values exceeding yield strength occurred (shown in gray color). This reveal that stress values > 338 MPa existed at: sharp edge (fig. 3.41); at wheel hole (fig. 3.42); at corners of hole profiles (fig. 3.43); at bend in steel plate (fig. 3.44). These areas would imply that changes are required in the design. These areas will be discussed in section 4.2.2.

3.7.2 Analysis of additive manufacture design

The investigation of stresses in the traditional design were done in similar way for the AM design. Areas of stress values > 338 MPa was also observed in this model, but to a lesser extent compared to what was seen in analysis of the traditional design. Max stress was was located at same place as the traditional design (fig. 3.45). Mesh was refined at this area to investigate in similar way to what was done in section 3.7.1. The data is presented in fig. 3.46. It is not quite clear if stresses at corner exceeds yield strength, but the author estimates it does. Other areas of interest regarding > 338 MPa stress is: at the truss-like features on top of section (fig. 3.47 and fig. 3.48) and at sharp edge (fig. 3.49). These areas will be discussed in section 4.2.3.
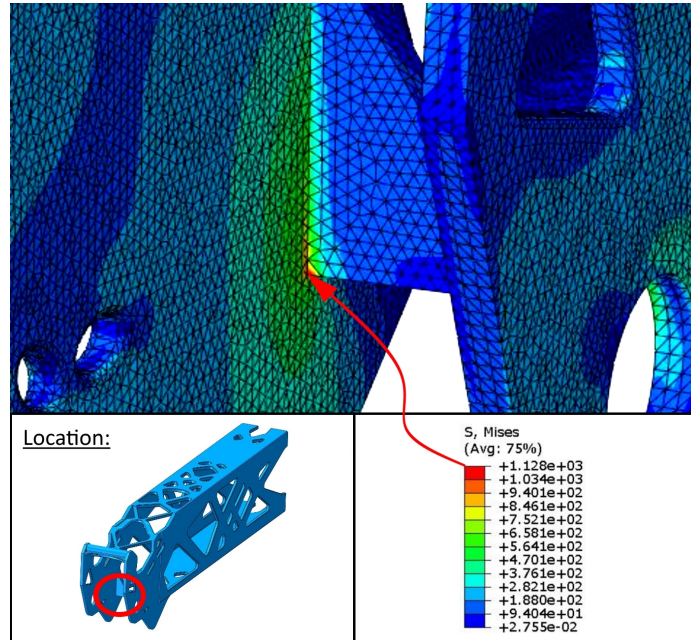
Figure 3.38: Maximum Von Mises Stress observed in traditional design.
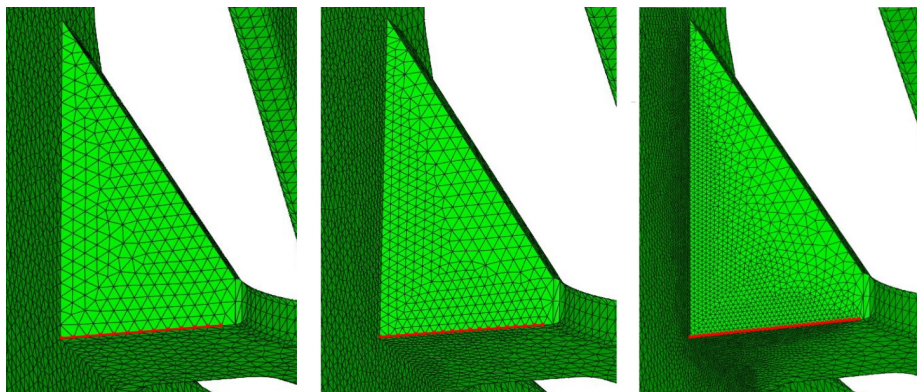
Figure 3.39: Mesh refining at corner. From the left: seed≈3 mm; seed≈2 mm; seed≈1 mm.
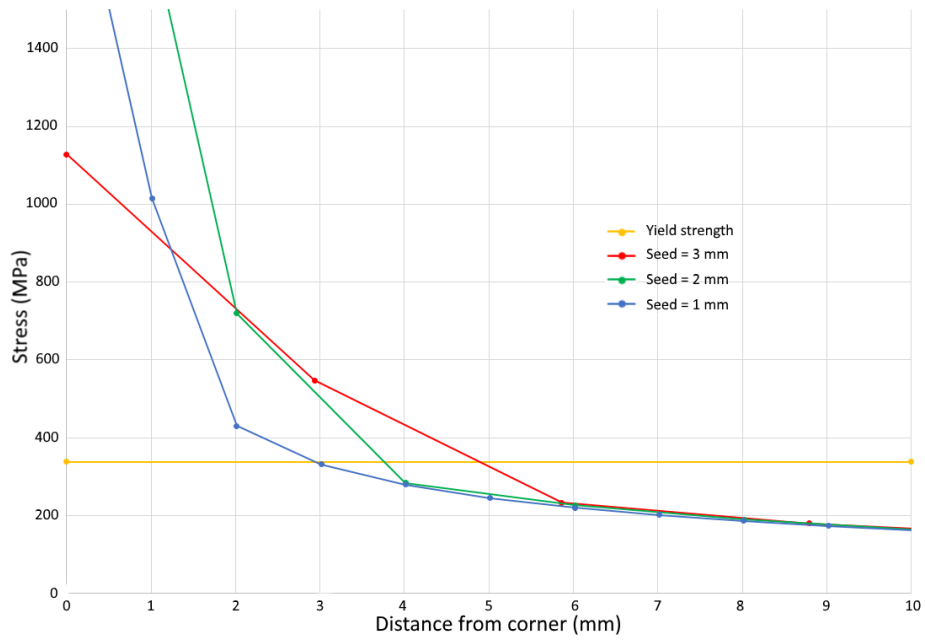
Figure 3.40: Traditional design: plot of stress at sharp corner shown in fig. 3.38 of different seed values.
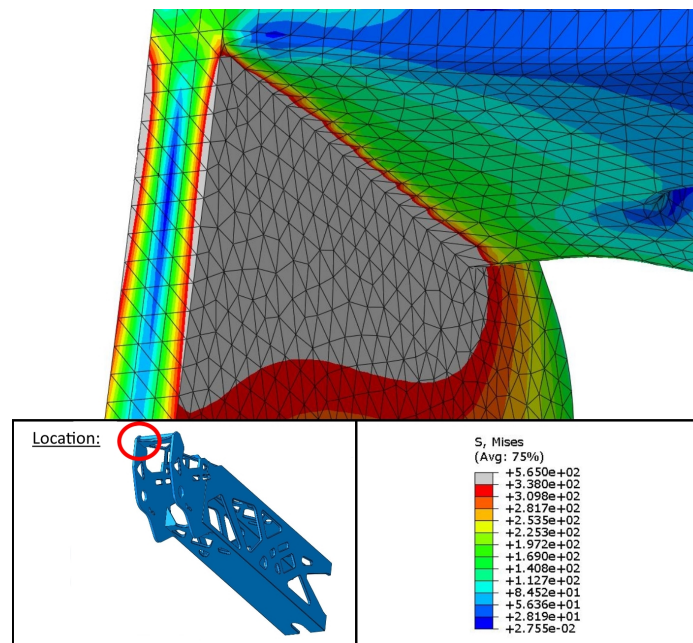
Figure 3.41: Traditional design: high stress values at sharp edge.
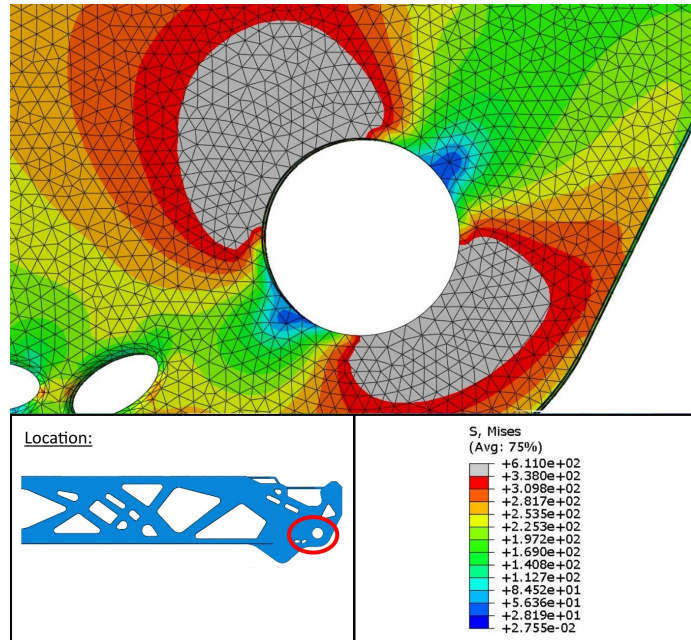
Figure 3.42: Traditional design: high stress values at wheel hole.
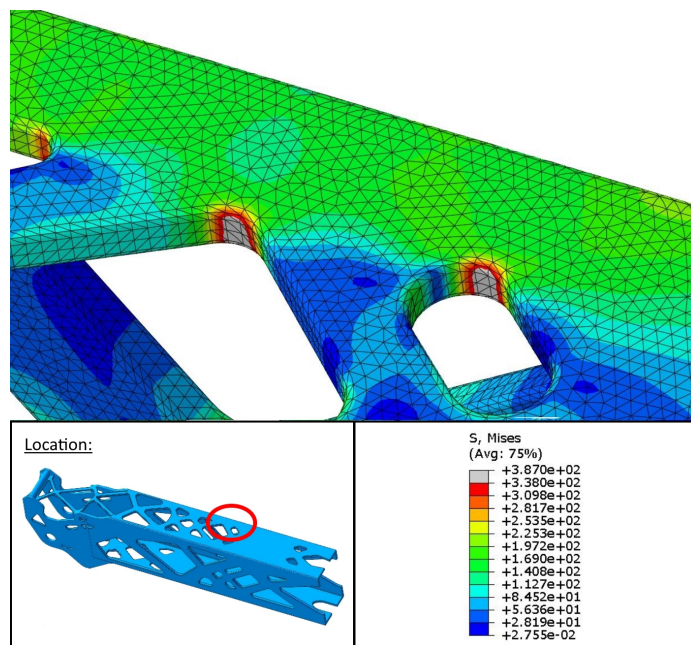
Figure 3.43: Traditional design: high stress values at corners of hole profiles.
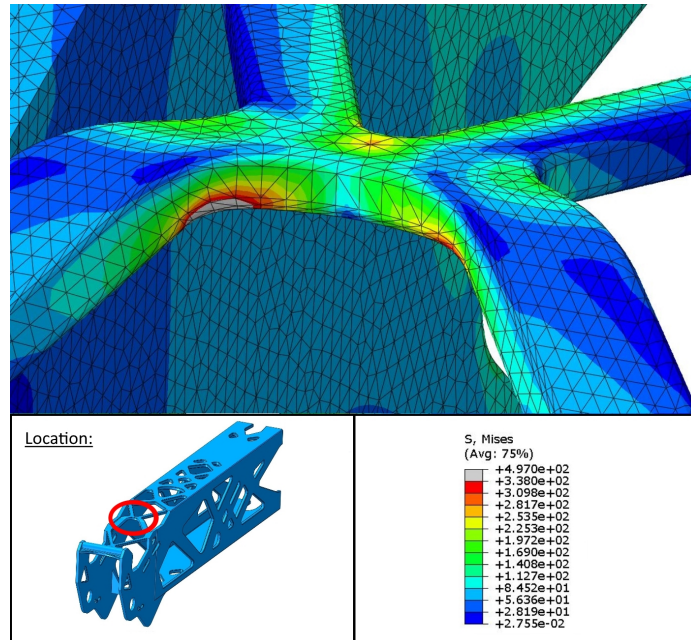
Figure 3.44: Traditional design: high stress values at bend in steel plate.
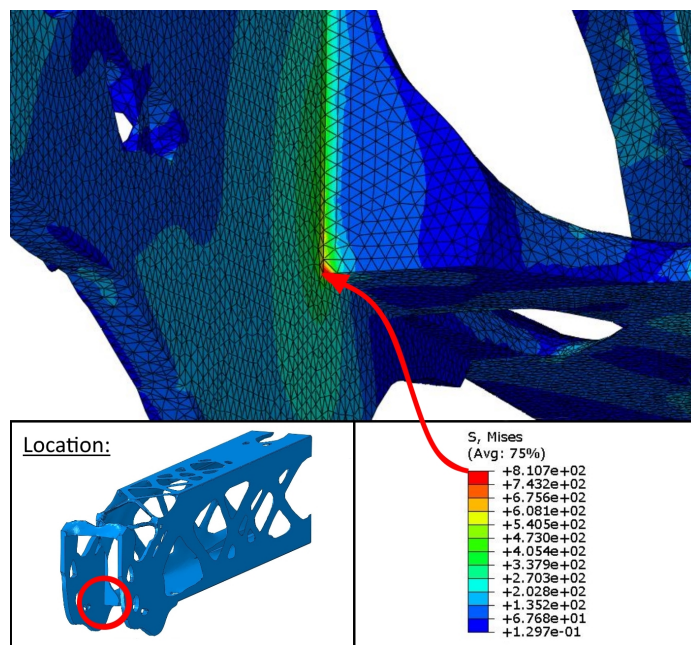
Figure 3.45: AM design: maximum Von Mises stress.
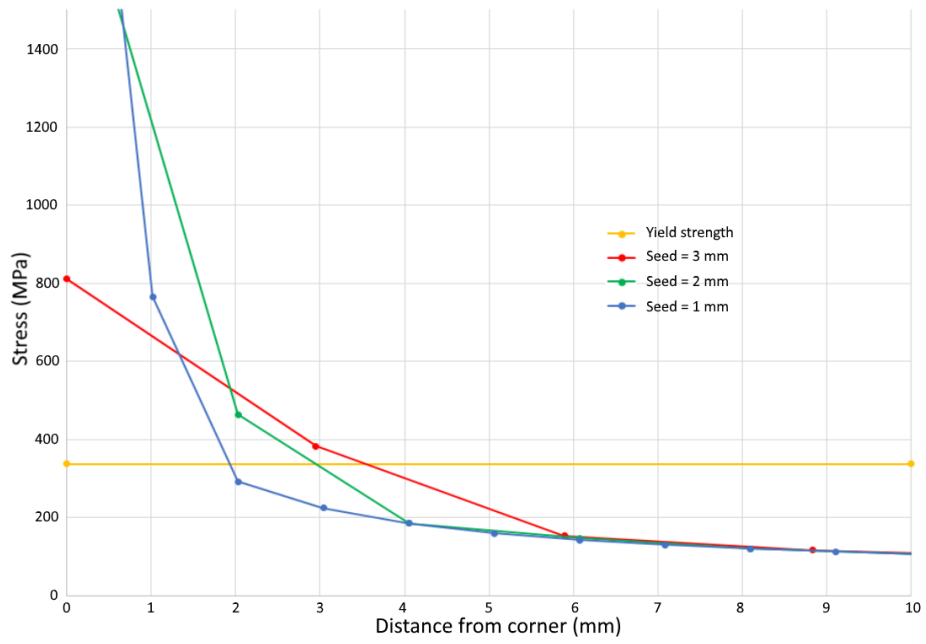
Figure 3.46: AM design: plot of stress at sharp corner shown in fig. 3.45 of different seed values.
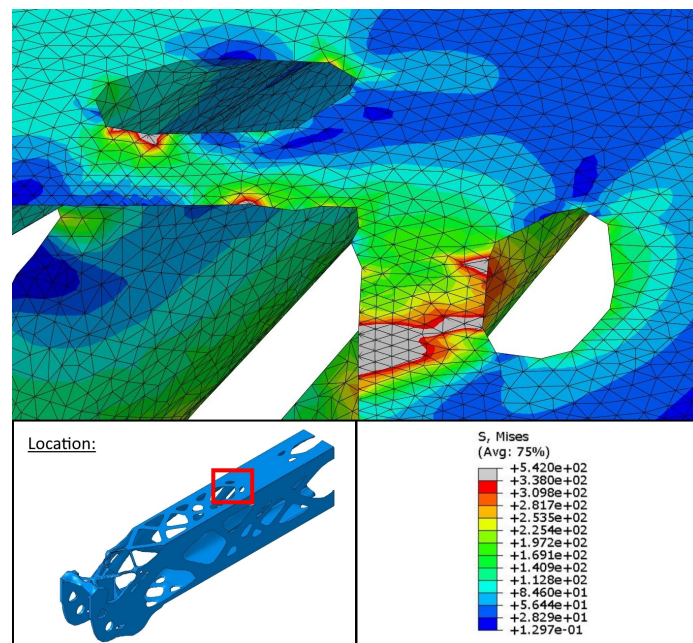
Figure 3.47: AM design: high stresses at truss-like features (from above).
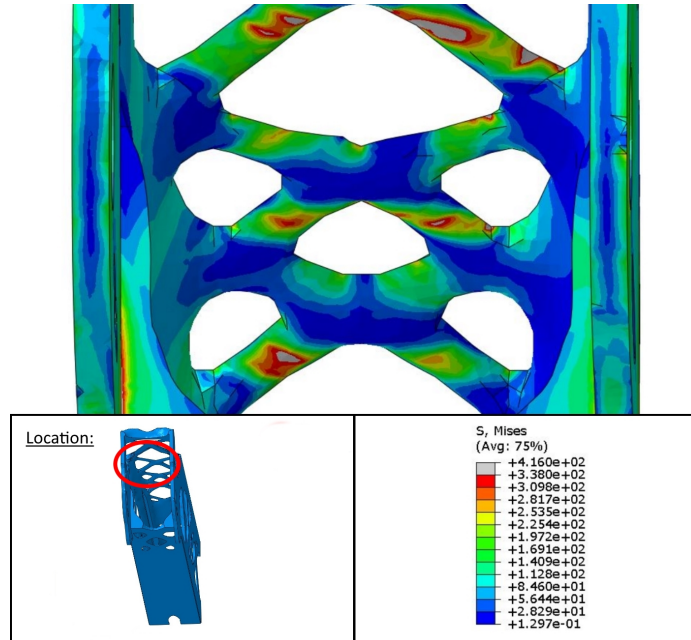
Figure 3.48: AM design: high stresses at truss-like features (from below).
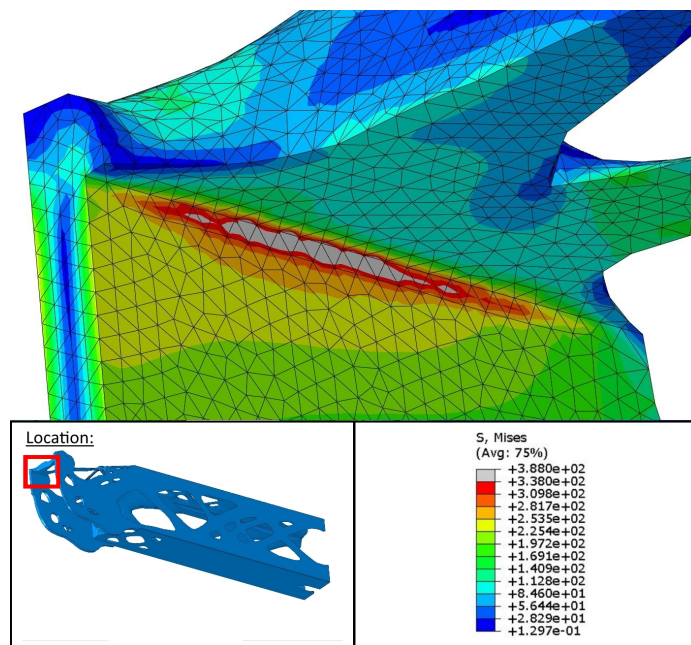
Figure 3.49: AM design: high stresses at sharp edge.

Chapter 4

Discussion

4.1 Pre-analysis

4.1.1 Design space

The limitations and rules set for defining the outer boundaries of the design space could have been chosen differently. In this thesis, the dimensions of the original component was used as a guide, with widths and heights of sections largely being equal to original measurements. This sort of similarity between original shape and shape of design space might not be useful.

Changes to the design space were made after test runs of topology optimization (as mentioned in section 3.3.2) showed that material was kept at the extremities of the design space. Such changes could have been done to a greater extent than what was done in this thesis. It is in the author's opinion that if material is kept at design space's outer limits after a topology optimization, it should be viewed as a sign that the design space is to restrictive, and ought to be expanded if this does not interfere with other physical objects (like a wheel or other parts of the assembly). One should also keep in mind that expanding design space would result in larger meshes, if element size is kept unchanged, so computational demand would also be of consideration in this matter.

4.1.2 Load case

Only one load case was considered in the analyses. Although the loads were quite conservative for this load case, it could have been beneficial to include more cases, especially when the min-max formulation of topology optimization allow for several load cases to be considered in one optimization. A minimum compliance topology optimization would only minimize compliance to the loads present, so having several load cases could result in more robustness in design.

4.1.3 Application of loads in FE-model

The way loads were assign to the FE-model was largely based on intuition by the author. A load was initially given by TKS as load on wheel, which would then be applied to the end truck via the wheel holes (or side plates in the case of the lateral loads). A more in-depth analysis on how the loads transfers from

wheel to end truck could have been done to get a better model of the actual
load situation.

4.1.4 Meshing

Given the level of detail required to create topologies that would utilize the
capabilities of 3D-printers combined to the relative large size of the total com-
ponent, it proved a challenge to develop a mesh that would keep computation
time at a reasonable low. Especially with quadratic elements.

Efforts were done to reduce size of the design space by studying initial test
runs of topology optimization and cutting away sections where material were
consequentially removed. More work could have been done on this matter, but
this reduces solution space of optimization and should be done with care. One
could also assume more direct control of the meshing algorithm and identify
areas where mesh should either be refined or made more coarse to increase
efficiency in element distribution, but a more coarse mesh might not be able to
represent the topologies to a satisfactory level of detail.

4.1.5 Setup of topology optimization

A minimization of compliance was considered as objective function for all topol-
ogy optimizations. Other formulations for objective function could be of inter-
est, such as maximization of eigenfrequency for dynamic analyses.

Implementing manufacturing constrains could have been used in an effort to
obtain topologies viable for traditional manufacture directly. However, as Liu
and Ma [5] points out in their review; while manufacturing-oriented topology
optimization have produced geometries with manufacturability, other, usually
greater, concerns such as manufacturing time and cost are rarely taken into
account in the optimization routines. The author would argue that this fact
would cause the resulting topologies to be reviewed and most likely edited by
an engineer anyway, so these constraints might not be worthwhile.

4.2 Results

4.2.1 Yield criterion

With the absence of a volume reduction goal prior to topology optimization,
a criteria for choosing a potentially viable topology was needed. The general
yield criterion from clause 6.2.1(5) in NS-EN 1993-1-1:2008 was used. This was
because of the varying cross section in the geometries, making standard capacity
checks by interaction of axial, moment and shear cross sectional resistances hard
to conduct. There is a note about clause 6.2.1(5) stating:

> The verification according to (5) can be conservative as it excludes
> partial plastic stress distribution, which is permitted in elastic de-
> sign. [43]

Given the lack of standardization for dealing with the unconventional geometries
produced by topology optimization for load bearing purposes, this conservative
approach was deemed appropriate. However, with further development of ad-
ditive manufacturing technologies for production of load bearing component

in steel, such as WAAM (section 2.3), there will be a need for more specialized standards for dealing with more complex load bearing geometries in the author's opinion.

No info was found regarding guidelines for material safety factors on maraging steel produced through WAAM. Therefore, the topology chosen after the yielding check in fig. 3.30 was used in design of both the traditional and the AM design. Relative to material strength of maraging steel (930 MPa according to [48]), this approach would indirectly represent a material factor for maraging steel of about:

$$\frac{f_{y,maraging}}{f_{y,355}/\gamma_{M0}} = \frac{930}{355/1,05} \approx 2,75$$

for the AM design.

4.2.2 Traditional design

The work of creating a conceptual design for traditional manufacture from the geometry of topology optimization was mainly done by intuition of the author. The modeling functionality of Inventor provided a basic guideline for what could be achieved by traditional manufacturing processes. The author's main academic background is in structural engineering and knowledge in capabilities of machining processes is limited, but, in the author's opinion, the model presented in this thesis is a fair first draft of design. Every profile of inner and outer boundaries in the model is defined with exact dimensions.

The static analysis validation of design showed some areas where Von Mises stress exceeded yield strength, like fig. 3.43 and fig. 3.44. This could be improved with slight alterations to profile dimensions, like increasing radii of curves were level of stress is an issue. The traditional design obtained a higher volume reduction compared to the AM design (which is almost identical to the extracted geometry from topology optimization), which could imply that too much liberty was taken when drafting the design in Inventor.

In analysis, the model was one solid, while in reality the design would be comprised by several components welded together. Welds were not modeled in the design. High stresses were located at areas where fillet welds were intended. Welds would have to be designed and studied further to evaluate if the stresses residing in these areas are critical or not. Strengthening these areas with additional brackets, might also be an option, keeping in mind the dimensions of the wheel to avoid interference.

4.2.3 AM design

The AM design was near equal to the exported STL geometry. When exporting the geometry from topology optimization to a STL-file, quite thin members (down to < 5 mm thickness) were observed, which were not that obvious when viewing the geometry as it appeared in the visualization module in Abaqus (see fig. 3.31). The difference observed were attributed to the smoothing algorithm in the STL extract function in Abaqus, and the author speculates if a finer mesh could perhaps prevent the extent of this phenomena. Some remodeling was done to the geometry regarding thin members, and more work could have been done on this matter.

Thin members raises concerns regarding vulnerabilities towards cyclic loads (fatigue) and local buckling. Additional analysis would be required to check if these features have to be changed to control these failure modes. One could also try to prevent formation of thin members in the first place by defining member size constraints in setup of the topology optimization.

The validation of design mainly showed acceptable stress levels, with some exceptions. There were located at rather thin truss-like members and at sharp corners. With additive manufacturing the component could be created as one solid (no need for welding, or attachment of any other kind, of separate parts). Taking this into account, the sharp corners of the model could be filleted in an effort to relive stresses residing at the corners (taking care that there still is sufficient space for the wheel). Slight alterations to the truss-like members, like increasing the thickness, could also improve stresses in these areas.

4.2.3.1 Comment about the AM design in relation to WAAM

Through the work of doing a literature study of the WAAM technology, knowledge was gained about this method that, to some degree, contradicted what was assumed by the author prior to this work. It was assumed by the author that AM processes had great capabilities of manufacturing components with complex geometry, and while that may be true for powder-bed and powder-fed systems, it was learned that WAAM systems did not have this quality to the same degree. As presented in section 2.3.6, there are design considerations that should be taken to achieve a successful manufacture with the WAAM process. Applying these considerations to the AM design presented in 3.6.3 have not actively been done since this was knowledge gained in the process of working with this thesis. With that said, it is in the authors opinion, based on what was learned in the literature study of WAAM, that the design presented for AM in this thesis could be viable for production with WAAM without drastic alterations. Also, the WAAM technology is still in it's infancy, with no commercial out-of-chamber[1] systems available at this moment. With that in mind, further development of WAAM might improve it's flexibility regarding the production of more complex geometries.

---

[1]Systems not contained within an inert gas chamber, able to produce large components (see section 2.3.3).

Chapter 5

Conclusion and further work

5.1 Summary

5.1.1 Literature study

A literature study was done to get a better foundation for decision making on how to approach this task, in terms of what methods are available in commercial software, which methods are most commonly used and why this is. The SIMP approach was found to be heavily favored in commercial software. The theory behind SIMP was studied and presented to provide better understanding when choosing parameters in the setup of the topology optimization.

The literature study also included a basic study of the WAAM method of 3D-printing metal components. Topology optimization and additive manufacturing are to research fields with the possibility of great synergy, and the WAAM method was of particular interest for TKS. It revealed that the WAAM method differentiated itself from other additive manufacturing methods. The level of detail and complexity often associated with 3D-printer's manufacturing capabilities, were more restricted with WAAM. Main advantage of WAAM have been listed as: high material efficiency, high deposition rate and that the process not necessarily have to be contained within a chamber, resulting in being able to produce larger components than other AM methods.

5.1.2 Topology optimization

This thesis have had a main focus on the task of performing a topology optimization. TKS provided a component which would undergo topology optimization. The component was the load bearing structure of a end truck in a overhead crane system (fig. 3.3). A design space was derived from this component, from which material would be removed and create a new topology. The topology optimization objective was be to minimize strain energy under a series of volume constraint. Five optimization were performed, each representing different levels of volume reduction from volume of original component (0%, 10%, 20%, 30% and 40%).

From the topology optimization, two conceptual design were created: one intended to be manufactured by traditional means and one intended to be manufactured by AM technology. The topology used as guideline for this design

was selected by checking (at a decided critical point) the results from the optimization runs against the general yield criterion given in NS-EN 1993-1-1:2005 (Eurocode 3) clause 6.2.1. The topology with most volume reduction who also satisfied yield criterion was chosen, and was found to be the 20% volume reduction topology.

Finally, a standard static analysis was performed on the two designs as a basic validation step. Von Mises stress values were investigated.

5.2 Conclusion

The main focus of this thesis have been to conduct a topology optimization of a crane component provided by TKS. The component was the load bearing parts of an end truck in a overhead crane system. The aim was to obtain a geometry to be used as a starting point for the creation of two conceptual designs; one intended for traditional manufacturing and one intended for additive manufacturing. To provide a better foundation of knowledge in performing topology optimization, a literature study was done on topology optimization methods in commercial software. It was also of interest for TKS to gain more knowledge about the WAAM technology, being a promising AM method for producing large load bearing steel components. Therefore, a literature study of WAAM method was done as well.

The most prominent topology optimization method used in commercial software was found to be the SIMP method, relating to the relative simplicity of the method, combined with the ability to yield good results for a wide range of problems.

The WAAM method differentiate itself from other AM method. WAAM is not quite as flexible for producing components with complex geometry, but the process don't have to be confined within a chamber, making it able to produce large components (meter scale). WAAM is also highly efficient in material usage (up to 100%) and wire material is relatively cheap compared to metal powder. Arc welding is also more energy efficient compared to laser or electron beam. WAAM is still in early development as a production method and guidelines for use is not available yet.

The five topology optimizations, with different volume constraints, produced clear, continuous geometries. The employment of the general yield criteria from NS-EN 1993-1-1:2008 on a assumed critical point on each topology optimization show that 20% volume reduction relative to original component was achievable. The corresponding geometry was exported in STL format and successfully used as a guideline to create a conceptual design for traditional design in Inventor. The Inventor add-in, Mesh enabler, proved useful in converting the STL file to a 3D model that was editable in Inventor, making it possible to implement changes to refine the design for additive manufacture. The final design intended for traditional manufacture had a volume reduction of 17%, while the design for AM manufacture had a volume reduction of 14% compared to the volume of the original component.

Static analysis of both designs showed Von Mises stress values that were above yield strength. Using linear hexahedron elements in topology optimization and the following yield check, while using quadratic tetrahedron elements in the static analysis validation, with a finer mesh, is most likely cause of the

observed difference in stress levels. Using same meshing strategy for topology optimization and the following validation would be preferred for better comparability. Tetrahedral meshing is recommended since the auto meshing with tetrahedral elements is more flexible and can handle the more complex geometries produced by topology optimization.

Improvements to the designs were discussed and it is believed that a viable design can be achieved without drastic alterations to the designs presented in this thesis. Topology optimization is a powerful tool in the conceptual stage of design. With improvements in topology optimization parameters and increased experience in using this tool, the road from topology optimization result to final, validated designs could become much shorter. This is especially true for design intended for additive manufacturing.

Further work

- Investigation into fatigue and buckling failure modes for thin members in the designs presented in this thesis..

- Determine dimensions of welds proposed for the traditional design to withstand the stresses residing at these locations.

- Refining profile dimensions and features for both designs to lower stresses.

- Investigation into the special considerations for designing with WAAM and how the AM design could be altered to accommodate this production method.

- Gain more knowledge about load transfer from wheel to end truck to develop more accurate representations of real load situation.

- Perform a topology optimization considering multiple load cases in an effort to obtain more robust geometries.

- Investigate if the mesh used in topology optimization can be improved, or computational power increased, to allow for a more refined mesh with quadratic elements.

Bibliography

[1] P. Keane. (Jun. 30, 2017). The new age of highly efficient products made with generative design, [Online]. Available: `https://www.engineering.com/DesignSoftware/DesignSoftwareArticles/ArticleID/15136/The-New-Age-of-Highly-Efficient-Products-Made-with-Generative-Design.aspx` (visited on 06/11/2018).

[2] Appliance Design. (Mar. 27, 2018). Report: 2018 sees dramatic rise in metal additive manufacturing and overall industry growth of 21%, [Online]. Available: `https://www.appliancedesign.com/articles/95804-report-2018-sees-dramatic-rise-in-metal-additive-manufacturing-and-overall-industry-growth-of-21` (visited on 06/06/2018).

[3] H. Eschenauer and N. Olhoff, "Topology optimization of continuum structures: A review", *Applied Mechanics Reviews*, vol. 54, no. 4, pp. 331–390, 2001. DOI: `10.1115/1.1388075`.

[4] G. Rozvany, "A critical review of established methods of structural topology optimization", eng, *Structural and Multidisciplinary Optimization*, vol. 37, no. 3, pp. 217–237, Jan. 2009, ISSN: 1615-147X.

[5] J. Liu and Y. Ma, "A survey of manufacturing oriented topology optimization methods", eng, *Advances in Engineering Software*, vol. 100, pp. 161–175, Oct. 2016, ISSN: 0965-9978.

[6] G. Rozvany, "Aims, scope, methods, history and unified terminology of computer-aided topology optimization in structural mechanics", *Structural and Multidisciplinary Optimization*, vol. 21, no. 2, pp. 90–108, Apr. 2001, ISSN: 1615-1488. DOI: `10.1007/s001580050174`. [Online]. Available: `https://doi.org/10.1007/s001580050174`.

[7] J. Deaton and R. Grandhi, "A survey of structural and multidisciplinary continuum topology optimization: Post 2000", *Structural and Multidisciplinary Optimization*, vol. 49, no. 1, pp. 1–38, 2014. DOI: `10.1007/s00158-013-0956-z`. [Online]. Available: `https://www.scopus.com/inward/record.uri?eid=2-s2.0-84892791680&doi=10.1007%2fs00158-013-0956-z&partnerID=40&md5=fa677158e95f2f851a4efe32974b4ffc`.

[8] O. Sigmund and K. Maute, "Topology optimization approaches: A comparative review", *Structural and Multidisciplinary Optimization*, vol. 48, no. 6, pp. 1031–1055, 2013. DOI: `10.1007/s00158-013-0978-6`. [Online]. Available: `https://www.scopus.com/inward/record.uri?eid=2-s2.0-84891011456&doi=10.1007%2fs00158-013-0978-6&partnerID=40&md5=90a9b6d6831641d91cff36ed4ebe8aa7`.

[9]   R. D. Cook, D. S. Malkus, M. E. Plesha, and R. J. Witt, *Concepts and applications of finite element analysis*, eng, 4th ed. New York: Wiley, 2002, ISBN: 0471356050.

[10] M. P. Bendsøe and O. Sigmund, *Topology optimization : theory, methods, and applications*, eng, Second Edition, Corrected Printing. Springer, 2004, ISBN: 3-662-05086-2.

[11] M. P. Bendsøe and N. Kikuchi, "Generating optimal topologies in structural design using a homogenization method", *Computer Methods in Applied Mechanics and Engineering*, vol. 71, no. 2, pp. 197–224, 1988, ISSN: 0045-7825. DOI: https://doi.org/10.1016/0045-7825(88)90086-2. [Online]. Available: http://www.sciencedirect.com/science/article/pii/0045782588900862.

[12] G. I. N. Rozvany, M. Zhou, and T. Birker, "Generalized shape optimization without homogenization", *Structural Optimization*, vol. 4, no. 3-4, pp. 250–252, Sep. 1992. DOI: 10.1007/bf01742754.

[13] Y. M. Xie and G. P. Steven, *Evolutionary Structural Optimization*. Springer-Verlag London, 1997. DOI: 10.1007/978-1-4471-0985-3.

[14] O. Sigmund, "A 99 line topology optimization code written in matlab", eng, *Structural and Multidisciplinary Optimization*, vol. 21, no. 2, pp. 120–127, Apr. 2001, ISSN: 1615-147X.

[15] D. Tcherniak and O. Sigmund, "A web-based topology optimization program", eng, *Structural and Multidisciplinary Optimization*, vol. 22, no. 3, pp. 179–187, Oct. 2001, ISSN: 1615-147X.

[16] G. Posch, K. Chladil, and H. Chladil, "Material properties of cmt-metal additive manufactured duplex stainless steel blade-like geometries", eng, *Welding in the World*, vol. 61, no. 5, pp. 873–882, Sep. 2017, ISSN: 0043-2288.

[17] Y. Saadlaoui, J.-L. Milan, J.-M. Rossi, and P. Chabrand, "Topology optimization and additive manufacturing: Comparison of conception methods using industrial codes", eng, *Journal of Manufacturing Systems*, vol. 43, pp. 178–186, Apr. 2017, ISSN: 0278-6125.

[18] D. Ding, Z. Pan, D. Cuiuri, and H. Li, "A multi-bead overlapping model for robotic wire and arc additive manufacturing (waam)", eng, *Robotics and Computer Integrated Manufacturing*, vol. 31, pp. 101–110, Feb. 2015, ISSN: 0736-5845.

[19] H. Lockett, J. Ding, S. Williams, and F. Martina, "Design for wire + arc additive manufacture: Design rules and build orientation selection", *Journal of Engineering Design*, vol. 28, no. 7-9, pp. 568–598, 2017. DOI: 10.1080/09544828.2017.1365826. eprint: https://doi.org/10.1080/09544828.2017.1365826. [Online]. Available: https://doi.org/10.1080/09544828.2017.1365826.

[20] X. Xu, S. Ganguly, J. Ding, S. Guo, S. Williams, and F. Martina, "Microstructural evolution and mechanical properties of maraging steel produced by wire + arc additive manufacture process", eng, *Materials Characterization*, 2017, ISSN: 1044-5803.

[21] B. Dunbar. (2012). Technology readiness level, [Online]. Available: `https://www.nasa.gov/directorates/heo/scan/engineering/technology/txt_accordion1.html` (visited on 02/15/2018).

[22] T. Artaza, A. Alberdi, M. Murua, J. Gorrotxategi, J. Frías, G. Puertas, M. Melchor, D. Mugica, and A. Suárez, "Design and integration of waam technology and in situ monitoring system in a gantry machine", *Procedia Manufacturing*, vol. 13, pp. 778–785, 2017. DOI: `10.1016/j.promfg.2017.09.184`. [Online]. Available: `https://www.scopus.com/inward/record.uri?eid=2-s2.0-85030850615&doi=10.1016%2fj.promfg.2017.09.184&partnerID=40&md5=3c4bdb4fa2a86b83ab7bb88cde3789dd`.

[23] S. W. Williams, F. Martina, A. C. Addison, J. Ding, G. Pardal, and P. Colegrove, "Wire + arc additive manufacturing", *Materials Science and Technology*, vol. 32, no. 7, pp. 641–647, 2016. DOI: `10.1179/1743284715Y.0000000073`. eprint: `https://doi.org/10.1179/1743284715Y.0000000073`. [Online]. Available: `https://doi.org/10.1179/1743284715Y.0000000073`.

[24] J. Ding, P. Colegrove, F. Martina, S. Williams, R. Wiktorowicz, and M. Palt, "Development of a laminar flow local shielding device for wire+arc additive manufacture", *Journal of Materials Processing Technology*, vol. 226, pp. 99–105, 2015, ISSN: 0924-0136. DOI: `https://doi.org/10.1016/j.jmatprotec.2015.07.005`. [Online]. Available: `http://www.sciencedirect.com/science/article/pii/S092401361530056X`.

[25] J. Ge, J. Lin, Y. Lei, and H. Fu, "Location-related thermal history, microstructure, and mechanical properties of arc additively manufactured 2cr13 steel using cold metal transfer welding", *Materials Science and Engineering: A*, vol. 715, pp. 144–153, 2018, ISSN: 0921-5093. DOI: `https://doi.org/10.1016/j.msea.2017.12.076`. [Online]. Available: `http://www.sciencedirect.com/science/article/pii/S0921509317316738`.

[26] H. Geng, J. Xiong, D. Huang, X. Lin, and J. Li, "A prediction model of layer geometrical size in wire and arc additive manufacture using response surface methodology", *The International Journal of Advanced Manufacturing Technology*, vol. 93, no. 1, pp. 175–186, Oct. 2017, ISSN: 1433-3015. DOI: `10.1007/s00170-015-8147-2`. [Online]. Available: `https://doi.org/10.1007/s00170-015-8147-2`.

[27] F. Youheng, W. Guilan, Z. Haiou, and L. Liye, "Optimization of surface appearance for wire and arc additive manufacturing of bainite steel", *The International Journal of Advanced Manufacturing Technology*, vol. 91, no. 1, pp. 301–313, Jul. 2017, ISSN: 1433-3015. DOI: `10.1007/s00170-016-9621-1`. [Online]. Available: `https://doi.org/10.1007/s00170-016-9621-1`.

[28] Amsterdam Institute for Advanced Metropolitan Solutions. (Sep. 29, 2017). Mx3d bridge update, [Online]. Available: `https://www.ams-institute.org/news/mx3d-bridge-update/` (visited on 02/24/2018).

[29] J. Prado-Cerqueira, J. Diéguez, and A. Camacho, "Preliminary development of a wire and arc additive manufacturing system (waam)", *Procedia Manufacturing*, vol. 13, pp. 895–902, 2017, ISSN: 2351-9789. DOI: `https://doi.org/10.1016/j.promfg.2017.09.154`. [Online]. Available: `http://www.sciencedirect.com/science/article/pii/S2351978917307916`.

[30] C. G. Pickin and K. Young, "Evaluation of cold metal transfer (cmt) process for welding aluminium alloy", *Science and Technology of Welding and Joining*, vol. 11, no. 5, pp. 583–585, 2006. DOI: 10.1179/174329306X120886. eprint: https://doi.org/10.1179/174329306X120886. [Online]. Available: https://doi.org/10.1179/174329306X120886.

[31] D. Ding, Z. Pan, D. Cuiuri, H. Li, S. van Duin, and N. Larkin, "Bead modelling and implementation of adaptive mat path in wire and arc additive manufacturing", *Robotics and Computer-Integrated Manufacturing*, vol. 39, pp. 32–42, 2016, ISSN: 0736-5845. DOI: https://doi.org/10.1016/j.rcim.2015.12.004. [Online]. Available: http://www.sciencedirect.com/science/article/pii/S0736584515301629.

[32] X. Xiong, H. Zhang, and G. Wang, "Metal direct prototyping by using hybrid plasma deposition and milling", *Journal of Materials Processing Technology*, vol. 209, no. 1, pp. 124–130, 2009, ISSN: 0924-0136. DOI: https://doi.org/10.1016/j.jmatprotec.2008.01.059. [Online]. Available: http://www.sciencedirect.com/science/article/pii/S0924013608000976.

[33] Y.-A. Song and S. Park, "Experimental investigations into rapid prototyping of composites by novel hybrid deposition process", *Journal of Materials Processing Technology*, vol. 171, no. 1, pp. 35–40, 2006, ISSN: 0924-0136. DOI: https://doi.org/10.1016/j.jmatprotec.2005.06.062. [Online]. Available: http://www.sciencedirect.com/science/article/pii/S0924013605006576.

[34] P. A. Colegrove, H. E. Coules, J. Fairman, F. Martina, T. Kashoob, H. Mamash, and L. D. Cozzolino, "Microstructure and residual stress improvement in wire and arc additively manufactured parts through high-pressure rolling", *Journal of Materials Processing Technology*, vol. 213, no. 10, pp. 1782–1791, 2013, ISSN: 0924-0136. DOI: https://doi.org/10.1016/j.jmatprotec.2013.04.012. [Online]. Available: http://www.sciencedirect.com/science/article/pii/S0924013613001416.

[35] H. Zhang, X. Wang, G. Wang, and Y. Zhang, "Hybrid direct manufacturing method of metallic parts using deposition and micro continuous rolling", *Rapid Prototyping Journal*, vol. 19, no. 6, pp. 387–394, 2013. DOI: 10.1108/RPJ-01-2012-0006. eprint: https://doi.org/10.1108/RPJ-01-2012-0006. [Online]. Available: https://doi.org/10.1108/RPJ-01-2012-0006.

[36] B. Panda, K. Shankhwar, A. Garg, and M. M. Savalani, "Evaluation of genetic programming-based models for simulating bead dimensions in wire and arc additive manufacturing", *Journal of Intelligent Manufacturing*, Nov. 2016, ISSN: 1572-8145. DOI: 10.1007/s10845-016-1282-2. [Online]. Available: https://doi.org/10.1007/s10845-016-1282-2.

[37] J. Xiong, G. Zhang, H. Gao, and L. Wu, "Modeling of bead section profile and overlapping beads with experimental validation for robotic gmaw-based rapid manufacturing", *Robotics and Computer-Integrated Manufacturing*, vol. 29, no. 2, pp. 417–423, 2013, ISSN: 0736-5845. DOI: https://doi.org/10.1016/j.rcim.2012.09.011. [Online]. Available: http://www.sciencedirect.com/science/article/pii/S0736584512001147.

[38] X. Lu, Y. F. Zhou, X. L. Xing, L. Y. Shao, Q. X. Yang, and S. Y. Gao, "Open-source wire and arc additive manufacturing system: Formability, microstructures, and mechanical properties", *The International Journal of Advanced Manufacturing Technology*, vol. 93, no. 5, pp. 2145–2154, Nov. 2017, ISSN: 1433-3015. DOI: 10.1007/s00170-017-0636-z. [Online]. Available: https://doi.org/10.1007/s00170-017-0636-z.

[39] W. E. Frazier, "Metal additive manufacturing: A review", *Journal of Materials Engineering and Performance*, vol. 23, no. 6, pp. 1917–1928, Jun. 2014, ISSN: 1544-1024. DOI: 10.1007/s11665-014-0958-z. [Online]. Available: https://doi.org/10.1007/s11665-014-0958-z.

[40] Ji, Lei, Lu, Jiping, Liu, Changmeng, Jing, Chenchen, Fan, Hongli, and Ma, Shuyuan, "Microstructure and mechanical properties of 304l steel fabricated by arc additive manufacturing", *MATEC Web Conf.*, vol. 128, p. 03006, 2017. DOI: 10.1051/matecconf/201712803006. [Online]. Available: https://doi.org/10.1051/matecconf/201712803006.

[41] O. Yilmaz and A. A. Ugla, "Microstructure characterization of ss308lsi components manufactured by gtaw-based additive manufacturing: Shaped metal deposition using pulsed current arc", *The International Journal of Advanced Manufacturing Technology*, vol. 89, no. 1, pp. 13–25, Mar. 2017, ISSN: 1433-3015. DOI: 10.1007/s00170-016-9053-y. [Online]. Available: https://doi.org/10.1007/s00170-016-9053-y.

[42] H. Bhadeshia and R. Honeycombe, "Chapter 13 - weld microstructures", in *Steels: Microstructure and Properties (Fourth edition)*, H. Bhadeshia and R. Honeycombe, Eds., Fourth edition, Butterworth-Heinemann, 2017, pp. 377–400, ISBN: 978-0-08-100270-4. DOI: https://doi.org/10.1016/B978-0-08-100270-4.00013-5. [Online]. Available: https://www.sciencedirect.com/science/article/pii/B9780081002704000135.

[43] Standard Norge, *Eurokode 3: Prosjektering av stålkonstruksjoner = eurocode 3: Design of steel structures. part 1-1: General rules and rules for buildings : Del 1-1 : Allmenne regler og regler for bygninger*, eng, Lysaker: Standard Norge, 2008.

[44] Dassault Systèmes, *Simulia user assistance 2017*, 2016.

[45] S. Johnsen, *Structural topology optimization: Basic theory, methods and applications*, nor, Johnsen, Steffen, 2013.

[46] K. A. James, J. S. Hansen, and J. R. Martins, "Structural topology optimization for multiple load cases using a dynamic aggregation technique", *Engineering Optimization*, vol. 41, no. 12, pp. 1103–1118, 2009. DOI: 10.1080/03052150902926827. eprint: https://doi.org/10.1080/03052150902926827. [Online]. Available: https://doi.org/10.1080/03052150902926827.

[47] A. Davis. (Oct. 14, 2014). Layer-by-layer: The evolution of 3-d printing, Ieee member charles hull invented the original process in 1983, [Online]. Available: http://theinstitute.ieee.org/tech-history/technology-history/layerbylayer-the-evolution-of-3d-printing (visited on 05/23/2018).

[48]   APWorks, *Material data sheet - maraging steel 1.2709 (ms1)*, May 7, 2017.
[Online]. Available: `http://www.apworks.de/en/wp-content/uploads/`
`sites/2/2015/07/20170705_STEEL_1.2709_REV0010.pdf` (visited on
05/30/2018).

Appendix A

Data from TKS

A.1   Load data

(Next page)

A.1.1 According to DIN 4132, DIN 15018 and FEM

CRANE WHEEL LOAD DATA

WHEEL LOADS ARE BASED ON PROPOSED GIRDER (AND SERVICE PLATFORM) WEIGHT

1 Wheel load drawing
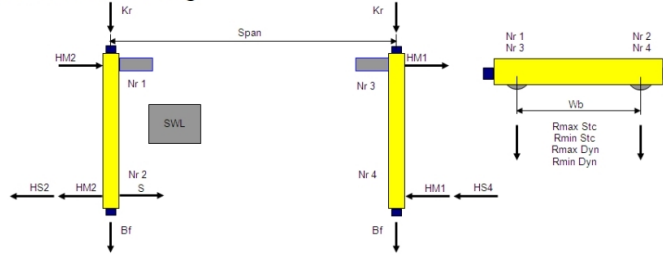
2 Crane information

Crane type	VTS10t x 14m Hol:6m	Buffer type	D2240
Span (Spa)	14,000 m	Wheel base (Wb)	2 500 mm
Load (SWL)	10 000 kg	Crane rail in calculation	FL60*40
Crane group	FEM A3	Wheel groove	74 mm
Crane speed	32/8 m/min		
Crane weight	4 490 kg	Crane travel limit switch	2-step

3 Hoist information

Hoist	Hoist type	Hoist group	Hoisting speed
Hoist 1 Main	VT304115R30DFP5	ISO M5	5/0,83 m/min
Hoist 1 Aux			

4 Vertical wheel loads

Wheel	NR1	NR2	NR3	NR4
Rmax Stc	59,7 kN	59,9 kN	-	-
Rmin Stc	-	-	11,5 kN	12,1 kN
Rmax Dyn	63,8 kN	64,0 kN	-	-
Rmin Dyn	-	-	12,5 kN	13,2 kN

5 Horizontal wheel loads (according to DIN 4132 + 15018 and FEM)

5.1	Inertia forces (from driving mechanisms)	HM1 = 1,7 kN	HM2 = 8,3 kN
5.2	Max. Wheel loads along each crane runway		Kr = 1,5 kN
5.3	Buffer force for dimensioning the crane runway end stop		Bf = 28 kN
5.4	Forces coming from skewing		
5.4.1	Guiding (contact) force (S= HS2 + HS4)		S = 19,9 kN
5.4.2	Friction forces due to oblique travel	HS2 = 16,5 kN	HS4 = 3,4 kN

Note! The inertia forces are acting on the crane structure only during acceleration and deceleration of the crane movement. Inertia forces and guiding forces do not act simultaneously. Guiding force S can also locate in wheel NR4.

A.1.2 According to ASCE 7 & AISC 7

Wheel loads according to ASCE 7 & AISC 7

Calculation number / work number	Test for Thomas - 10000kg /
Rated capacity of crane	10 000 kg
Span	14,000m
Wheel base	2 500mm
Rail type / Wheel groove width	FL60*40 / 74mm
Classification of crane use as a whole	A3

Trolley position closest to Rail 1

ASCE7 4.9.2 Maximum static vertical wheel loads

	Rail 1	Rail 2
Wheel I,1, $F_{z,I,1}$	-59,6 kN	-11,6 kN
Wheel I,2, $F_{z,I,2}$	-59,8 kN	-12,2 kN

ASCE7 4.9.3 Maximum dynamic vertical wheel loads
(With impact factor 110 %)

	Rail 1	Rail 2
Wheel I,1, $F_{z,,impl,1}$	-65,6 kN	-12,7 kN
Wheel I,2, $F_{z,,impl,2}$	-65,7 kN	-13,5 kN

ASCE7 4.9.5 Longitudinal Force

	Rail 1	Rail 2
Side I, $F_{y,I}$	11,9 kN	2,32 kN

AISC7 13.4 Bumper Force

	Rail 1	Rail 2
Bumper I, $F_{b,I}$	18,8 kN	14,8 kN

ASCE7 4.9.4 Lateral force, $F_{x,tot}$ = 20,9 kN
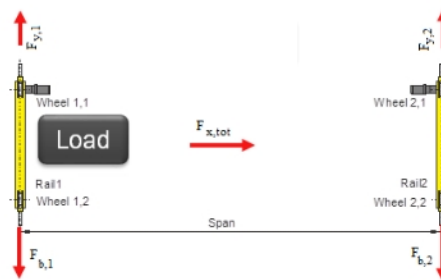
Trolley position closest to Rail 2

ASCE7 4.9.2 Maximum static vertical wheel loads

	Rail 1	Rail 2
Wheel I,1, $F_{z,I,1}$	-11,5 kN	-59,7 kN
Wheel I,2, $F_{z,I,2}$	-12,1 kN	-59,9 kN

ASCE7 4.9.3 Maximum dynamic vertical wheel loads
(With impact factor 110 %)

	Rail 1	Rail 2
Wheel I,1, $F_{z,,impl,1}$	-12,6 kN	-65,7 kN
Wheel I,2, $F_{z,,impl,2}$	-13,3 kN	-65,9 kN

ASCE7 4.9.5 Longitudinal Force

	Rail 1	Rail 2
Side I, $F_{y,I}$	2,29 kN	11,9 kN

AISC7 13.4 Bumper Force

	Rail 1	Rail 2
Bumper I, $F_{b,I}$	14,8 kN	18,8 kN

ASCE7 4.9.4 Lateral force, $F_{x,tot}$ = 20,9 kN

Note! The inertia forces are acting on the crane structure only during acceleration and deceleration of the crane movement. Inertia forces and guiding forces do not act simultaneously. Guiding force S can also locate in wheel NR4.

The Component selection, wheel loading, motor data etc. are based on the proposed main girder weight, duty groups, cranes speeds and other technical details shown the Component Offer and other prints. Any changes to these values may change the crane components. All the technical information in this print is guiding and indicative only and therefore to be interpreted by experts only. This computer program is protected by copyright laws and international treaties.

A.2 Drawings

A.2.1 End truck
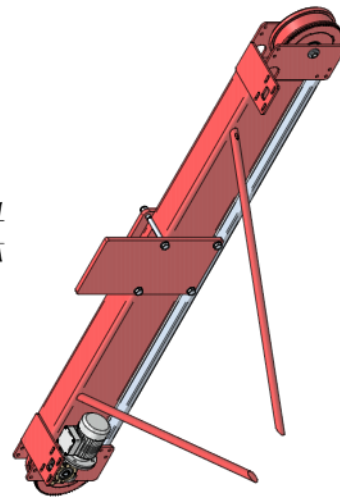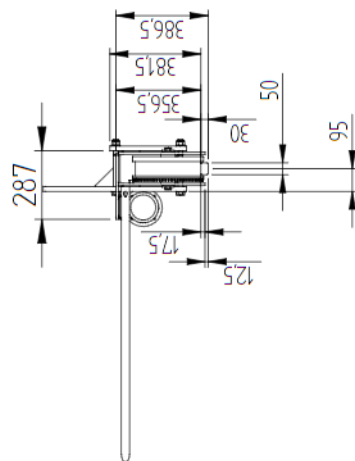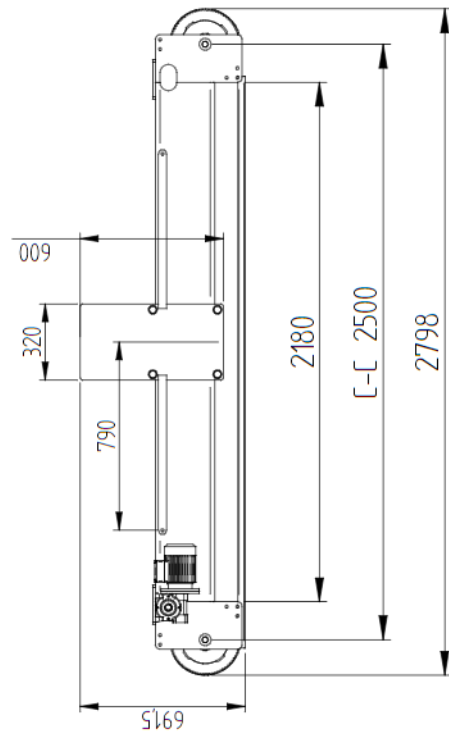
Appendix B

Data from analysis

B.1   Parameter data from topology optimizations

(Next page)

topo_opt_100

iteration	strain energy	volume	normalized volume
0	1602527	0,346	1,000
1	1037624	0,321	0,928
2	697684	0,334	0,964
3	535540	0,339	0,979
4	429138	0,340	0,984
5	348322	0,340	0,984
6	285327	0,339	0,979
7	236803	0,337	0,974
8	206485	0,340	0,983
9	173879	0,337	0,974
10	151661	0,336	0,972
11	136776	0,336	0,970
12	124854	0,339	0,980
13	114011	0,338	0,977
14	108629	0,340	0,983
15	104452	0,338	0,978
16	99269	0,341	0,986
17	95518	0,338	0,978
18	93691	0,340	0,982
19	90334	0,341	0,987
20	88318	0,342	0,988
21	86959	0,343	0,990
22	85872	0,343	0,992
23	85291	0,344	0,993
24	85055	0,343	0,992
25	84245	0,344	0,995
26	84163	0,344	0,995
27	83900	0,344	0,995
28	83459	0,345	0,997
29	83216	0,345	0,997
30	83210	0,345	0,996
31	82979	0,345	0,997
32	82955	0,345	0,997
33	82890	0,345	0,997
34	82731	0,345	0,998
35	82622	0,345	0,998
36	82622	0,345	0,997

topo_opt_090

iteration	strain energy	volume	normalized volume
0	2301402	0,312	0,901
1	1454956	0,287	0,828
2	954680	0,301	0,871
3	729800	0,306	0,883
4	578470	0,307	0,886
5	460807	0,306	0,885
6	368507	0,304	0,879
7	305411	0,304	0,880
8	249726	0,302	0,873
9	209870	0,301	0,870
10	182099	0,301	0,870
11	160744	0,304	0,879
12	145735	0,303	0,876
13	136499	0,307	0,887
14	127644	0,306	0,883
15	122465	0,309	0,892
16	114331	0,307	0,888
17	112558	0,305	0,881
18	109810	0,306	0,885
19	105937	0,307	0,888
20	102697	0,309	0,893
21	101206	0,309	0,893
22	99858	0,310	0,895
23	99136	0,310	0,896
24	98673	0,310	0,896
25	98077	0,310	0,897
26	97756	0,311	0,898
27	97569	0,311	0,898
28	97101	0,311	0,899
29	96933	0,311	0,899
30	96922	0,311	0,899
31	97050	0,311	0,898
32	96948	0,311	0,899
33	96784	0,311	0,899
34	96560	0,311	0,899
35	96499	0,311	0,899
36	96296	0,311	0,899

⋮

37	96253	0,311	0,899
38	96118	0,311	0,899
39	95895	0,311	0,900
40	95621	0,311	0,900
41	95527	0,311	0,900
42	95386	0,311	0,900
43	95406	0,311	0,900

⋮

topo_opt_080

Iteration	strain energy	volume	normalized volume
0	3490206	0,277	0,801
1	2143910	0,253	0,732
2	1381334	0,268	0,775
3	1049359	0,271	0,785
4	818719	0,272	0,786
5	637884	0,271	0,784
6	492081	0,269	0,777
7	395917	0,270	0,782
8	307443	0,268	0,773
9	259602	0,266	0,769
10	224832	0,273	0,789
11	197517	0,269	0,777
12	181099	0,273	0,790
13	167476	0,271	0,783
14	160688	0,273	0,789
15	155393	0,270	0,781
16	149018	0,270	0,782
17	140498	0,272	0,786
18	136165	0,272	0,785
19	129862	0,274	0,791
20	125731	0,274	0,792
21	123110	0,274	0,793
22	121012	0,275	0,794
23	119751	0,275	0,795
24	118879	0,275	0,795
25	117634	0,275	0,796
26	116942	0,275	0,796
27	116364	0,276	0,796
28	115642	0,276	0,797
29	115240	0,276	0,797
30	114958	0,276	0,797
31	114371	0,276	0,797
32	114227	0,276	0,797
33	114001	0,276	0,797
34	113654	0,276	0,798
35	113215	0,276	0,798
36	112975	0,276	0,797

⋮

37	112844	0,276	0,797
38	112608	0,276	0,797
39	112475	0,276	0,797
40	112264	0,276	0,798
41	111951	0,276	0,798
42	111606	0,276	0,798
43	111330	0,276	0,798
44	111309	0,276	0,798
45	111181	0,276	0,798
46	111164	0,276	0,798
47	110982	0,276	0,799
48	110927	0,276	0,799
49	110826	0,276	0,799
50	110894	0,276	0,798
51	110800	0,276	0,799
52	110678	0,276	0,799
53	110573	0,276	0,799
54	110325	0,277	0,799
55	110211	0,277	0,799
56	110163	0,276	0,799
57	110123	0,277	0,799

topo_opt_070

iteration	strain energy	volume	normalized volume
0	5599267	0,242	0,700
1	3357647	0,221	0,640
2	2127850	0,235	0,678
3	1596122	0,237	0,685
4	1220106	0,237	0,686
5	923116	0,236	0,682
6	675984	0,234	0,676
7	515800	0,234	0,677
8	402596	0,233	0,674
9	328292	0,234	0,678
10	281939	0,237	0,684
11	248283	0,235	0,680
12	228124	0,239	0,691
13	205389	0,238	0,688
14	198616	0,239	0,691
15	190729	0,237	0,684
16	180537	0,238	0,688
17	172335	0,238	0,688
18	165999	0,239	0,691
19	159446	0,239	0,692
20	155485	0,239	0,692
21	152340	0,240	0,692
22	148659	0,240	0,693
23	147221	0,240	0,693
24	146201	0,240	0,693
25	143606	0,240	0,693
26	142395	0,240	0,693
27	140489	0,240	0,694
28	139336	0,240	0,694
29	138526	0,240	0,695
30	137748	0,241	0,695
31	136977	0,241	0,696
32	136382	0,241	0,696
33	135891	0,241	0,696
34	135799	0,241	0,695
35	135134	0,241	0,696
36	134386	0,241	0,696

⋮

37	133834	0,241	0,696
38	133378	0,241	0,697
39	133107	0,241	0,697
40	133132	0,241	0,697
41	132853	0,241	0,697
42	132504	0,241	0,697
43	132132	0,241	0,697
44	132016	0,241	0,697
45	131797	0,241	0,697
46	131710	0,241	0,697
47	131638	0,241	0,697
48	131395	0,241	0,698
49	131258	0,241	0,698
50	131081	0,241	0,698
51	131152	0,241	0,698
52	131163	0,241	0,697

⋮

topo_opt_60

iteration	strain energy	volume	normalized volume
0	9507300	0,208	0,601
1	5631132	0,191	0,551
2	3498021	0,201	0,582
3	2564041	0,204	0,588
4	1909595	0,204	0,589
5	1377510	0,202	0,583
6	1013485	0,199	0,576
7	720486	0,200	0,578
8	553635	0,199	0,576
9	447439	0,204	0,589
10	376320	0,201	0,582
11	335431	0,205	0,594
12	292893	0,204	0,590
13	282799	0,204	0,590
14	274381	0,203	0,586
15	257597	0,204	0,589
16	239536	0,204	0,591
17	225740	0,205	0,594
18	214816	0,206	0,595
19	207065	0,206	0,595
20	200354	0,206	0,595
21	193695	0,206	0,596
22	189928	0,206	0,594
23	186879	0,206	0,594
24	182606	0,206	0,595
25	179195	0,206	0,594
26	175862	0,206	0,595
27	173161	0,206	0,596
28	171181	0,206	0,596
29	170076	0,206	0,596
30	168515	0,207	0,597
31	166566	0,207	0,598
32	164981	0,207	0,598
33	163744	0,207	0,598
34	163324	0,207	0,598
35	163152	0,207	0,598
36	162288	0,207	0,599

⋮

37	161427	0,207	0,599
38	161003	0,207	0,599
39	160783	0,207	0,599
40	160794	0,207	0,599
41	160836	0,207	0,599
42	160300	0,207	0,599
43	160084	0,207	0,599
44	159696	0,207	0,599
45	159470	0,207	0,599
46	159376	0,207	0,599
47	159393	0,207	0,599

⋮

79